Marine Pollution Bulletin 230 (2026) 119812

Contents lists available at ScienceDirect

Marine Pollution Bulletin

journal homepage: www.elsevier.com/locate/marpolbul

Droplet formation, drift, weathering, and natural dispersion in two North Sea experimental oil spills

Tor Nordam [a,b,*], Atle Kleven [a], Frode Leirvik [a], Liv-Guri Faksness [a], Per Johan Brandvik [a,b], Jørgen Skancke [a], Arsalan Mostaani [b], Gaute Hope [c], Trygve Halsne [c], Ingrid C. Taban [d], Kristin K. Husebye [d], John Inge Karoliussen [d], Ove Njøten [e], Knut-Frode Dagestad [c], Lars Robert Hole [c], David Peddie [f], Øyvind Breivik [c,g]

[a] *SINTEF Ocean, Trondheim, Norway*
[b] *Norwegian University of Science and Technology, Trondheim, Norway*
[c] *Norwegian Meteorological Institute, Bergen, Norway*
[d] *Norwegian Clean Seas Association for Operating Companies (NOFO), Stavanger, Norway*
[e] *Norwegian Coastal Administration, Horten, Norway*
[f] *Offshore Sensing, Bergen, Norway*
[g] *Geophysical Institute, University of Bergen, Bergen, Norway*

ARTICLE INFO

Keywords:
Marine oil spills
Droplet size distribution
Droplet formation
Natural dispersion
In-situ measurements

ABSTRACT

Accurate oil spill modelling is crucial for environmental risk assessment and operational preparedness for marine oil spills. Predicting drift, weathering, and droplet sizes in natural dispersion is essential. Existing droplet size models are fitted to laboratory results, and a lack of field data makes it uncertain how well these models apply in real conditions.

Here we show for the first time in situ measurements of droplet size distributions during natural dispersion in the field. Observations have been made from two controlled experimental spills of 10 m^3, each followed for 24 h. Droplet sizes were measured from a novel spar buoy with integrated silhouette camera. Supporting measurements included oil properties, wind, waves, currents, and hydrography, as well as remote sensing from multiple platforms. The data was collected during a field experiment conducted in the North Sea by NOFO in collaboration with the NCA. Two oil types were studied at two weather conditions. MGO released under calm wind (2–7 m/s) resulted in few droplets, and the slick remained thicker than expected, up to 8 mm after 24 h. Oseberg crude drifted in up to 12 m/s wind, with observed d_{50}^{v} in the range 90–1667 μm.

Previously published droplet size models were evaluated. While no model was clearly better in terms of absolute errors, the model by Johansen closely followed an observed trend of reduced droplet size at later times. These results provide the first direct field evidence to evaluate and constrain droplet size parameterizations for oil spill modelling.

1. Introduction

Marine oil spill modelling is an essential component in risk assessment for ocean-based oil and gas extraction as well as fuel and cargo spills from ships (Keramea et al., 2021; Nordam et al., 2017; Price et al., 2003). These models are also extensively used for oil spill response planning and to aid oil spill response in the event of a spill (Aamo et al., 1997; Barker et al., 2020; Liu et al., 2011). Oil spill models are mainly developed based on laboratory experiments (Delvigne and Sweeney, 1988; Reed et al., 2001; Johansen et al., 2015; Nordam et al., 2020), which make field data very valuable for both verification and further development. Observational data from accidental spills are usually not comprehensive, for reasons including the difficulty of establishing a measurement campaign on short notice, the priority usually being on the response, as well as in many cases adverse weather. In contrast to spills of opportunity, planned field experiments provide the opportunity to conduct planned and carefully controlled measurement campaigns developed specifically to, e.g., advance the state of the art of oil spill

* Corresponding author.
E-mail address: tor.nordam@sintef.no (T. Nordam).

https://doi.org/10.1016/j.marpolbul.2026.119812
Received 13 February 2026; Received in revised form 16 April 2026; Accepted 26 April 2026
Available online 7 May 2026

modelling.

Despite being relatively rare, field experiments have offered valuable knowledge both for general process understanding, verification of response technologies, and model development. Focus of past field experiments have included weathering and emulsification (Daling and Strøm, 1999; Daling et al., 2003), evaporation and dissolution (Harrison et al., 1975; Gros et al., 2014), and oil behaviour and response options in both open and ice-covered waters (Daling et al., 2002; Faksness et al., 2011). When available, field data has been invaluable for model development and validation, e.g. for weathering and emulsification (Daling and Strøm, 1999) and drift modelling (Reed et al., 1994; Röhrs et al., 2018).

Natural dispersion is a key process in the transport and fate of oil spilled at sea, affecting among other things dissolution, biodegradation, and horizontal dispersion (Johansen, 1982; Reed et al., 1994; Röhrs et al., 2018). In particular, the droplet size distribution produced by wave entrainment controls the vertical rise velocity, and thus the potential for the oil to form and remain as a surface slick. Natural entrainment is therefore an important process to describe in oil spill modelling, key to predicting, e.g., impacts to birds and mammals, as well as beaching. In addition, it has recently been pointed out that submerged oil droplets are typically overlooked in environmental risk assessments, and have significant potential to impact fish eggs (Frøysa et al., 2025).

Entrainment by breaking waves has been studied extensively in the lab by multiple groups, and several different droplet size models are published (see, e.g., Johansen et al., 2015; Li et al., 2017b, Wang et al., 2024, Mostaani et al., 2026b). The most widely used models are so-called equilibrium models, which are dimensionless correlations predicting a characteristic droplet size as a function of oil and wave properties. These are fitted to results from lab studies, typically with significant wave height as an input parameter. However, breaking waves in the lab and the field are not created by the same mechanisms, and wave heights used in lab studies with oil are much smaller than those that can be encountered in the field.

Dispersion has been studied in the field, both natural dispersion and with chemical dispersants (Cormack and Nichols, 1977; Delvigne, 1985), though droplet sizes have not been a major focus. Rather, concentrations of droplets and dissolved compounds have been measured by, e.g., laser scattering and fluorometer (Genders, 1988) or water sampling (Gros et al., 2014). Lunel (1993) and Jensen et al. (2008) measured droplets from a chemically dispersed oil slick, but to the best of our knowledge, droplet sizes from natural dispersion of an untreated slick have never been measured in situ. It is therefore of great interest to the community to obtain field data for natural entrainment to evaluate and improve on the previously published models.

1.1. Background and objectives of the study

Following the awareness raised regarding the fate of oil spilled at sea after the Ekofisk Bravo blowout in 1977, NOFO (Norwegian Clean Seas Association for Operating Companies) was established. Numerous field experiments with oil, called Oil On Water (OOW), have since been carried out in Norwegian waters (Faksness et al., 2016). These experiments are conducted by NOFO in collaboration with the Norwegian Coastal Administration (NCA), with a release permit granted by the Norwegian Environment Authority. The aim is to verify and further develop oil spill equipment and technologies, produce knowledge about oil spills and oil spill response among those who are responsible for oil spill contingency in Norway, and to provide data for model development and validation. For additional information, see the Supplementary materials, as well as Taban et al. (2025).

At OOW in June 2025, two experimental releases were carried out, one with a diesel-type refined fuel oil and one with a fresh crude. The first experiment released 10 m^3 of MGO (Marine gas oil). Due to a trend of shipping switching from heavier bunker fuels towards lighter, diesel-type fuels, there is an increased need of knowledge about the fate and behaviour of light distillates. The intention was specifically to study the spreading and evaporation of a diesel spill in calm conditions, with little or no breaking waves. A similar experiment in 2022 indicated that the diesel slick remained coherent with a thickness of several millimetres after 8 h (Karoliussen et al., 2022), which was longer than previously thought possible. This indicated that the window of opportunity for response to a diesel spill could be long enough for options such as mechanical recovery, chemical dispersion or in situ burning to be relevant, particularly in calm and cold conditions. It was therefore of interest to investigate if spills of diesel fuel can remain thick and combatable over even longer periods of time than the 8-hour duration of the experiment in OOW 2022. Objectives also included the need to evaluate a range of different remote sensing capabilities, including at night, for a transparent oil with limited own colour, and with known thickness from the surface sampling campaign.

The second experiment released 10 m^3 of fresh Oseberg crude oil in breaking wave conditions. The primary purpose was to study the natural dispersion process, and to collect a dataset of sufficient accuracy for model evaluation. Relying on newly developed measurement buoys (Cavaleri et al., 2025) we have sought for the first time to simultaneously measure both the parameters that droplet size models rely on (wave height, slick thickness, oil viscosity) and the resulting entrained droplet size distributions in the water column. Specifically the objective was to collect a comprehensive dataset to allow evaluation of published droplet size models, which are all based on lab data, against droplet size distributions in realistic field conditions.

1.2. Outline of this paper

The layout of the paper is as follows: In Section 2 we give an overview of the measurement campaign, describing the different instruments and techniques, and the measured parameters. In Section 3, we present and discuss the results, first for the MGO experiment, then for Oseberg crude oil. In Section 4 we discuss in detail the measured droplet size distributions during the Oseberg crude experiment, in the context of existing droplet size parameterisations from the literature. Finally, in Section 5 we present some concluding remarks.

2. Materials and methods

OOW 2025 was conducted on June 6 to June 9, 2025. The experimental area is located approximately 150 km to the west of Bergen, Norway, at the location of the Frigg gas field. Production at the field was closed in 2004, and infrastructure removal completed in 2010.[1] The water depth in the area is around 100 m. The field experiments were conducted from two vessels, the Norwegian Coast Guard vessel *Bergen* (NoCGV *Bergen*), and MS *Sunny Lady*. NoCGV *Bergen* was the command vessel and was used for release of oil. NoCGV *Bergen* was also fitted with a mobilizable dispersant application system according to the NOFO 2021 standard,[2] as well as oil spill response equipment for mechanical recovery. In addition, NoCGV *Bergen*, with its two work boats (Sjøbjørn 25, Mk. III) was the base of operations for all surface sampling and deployment of instruments to the sea. *Sunny Lady* had temporarily installed additional remote sensing equipment and was the base for all activity with Unmanned Aerial Vehicles (UAVs). In addition to the activities related to these vessels, a surveillance aircraft (LN-KYV) and satellites were used for remote sensing purposes throughout the experiments.

2.1. Meteorological and oceanographic observations

Meteorological and oceanographic observations were conducted to

[1] https://www.norskpetroleum.no/en/facts/field/frigg/.
[2] NOFO_standard_2021_-_english_version.pdf.

obtain the data needed by oil spill models to predict how different processes affect the transport and fate of the oil. For the Oseberg experiment, with a focus on droplet size distributions, particular emphasis was placed on the measurement of waves. Below we describe the most relevant observations for this study. Some additional details are given in Section 2 of the supplementary material.

2.1.1. Sailbuoy

Wind, temperature and air pressure were measured with a remotely piloted Sailbuoy (Hole et al., 2016), which was deployed a few hours prior to the start of the first experiment on June 6, and recovered a few hours after the end of the second experiment on June 9. The Sailbuoy was directed to maintain station a small distance away from the predicted trajectory of the oil to measure wind representative of the conditions at the slick. Note that the Sailbuoy measured wind at an elevation of 0.5 m. This was scaled with a logarithmic wind profile to 10 m height, which is the standard reference height for wind used by models. The scaling follows Brekke et al. (2021), where measured and scaled winds from the Sailboy were also compared to other sources, and found to be a good match.

2.1.2. Acoustic Doppler Current Profiler (ADCP)

A Nortek Signature 500 ADCP was deployed prior to the start of the first experiment. It was deployed with a bottom anchor and a buoyancy package positioning the ADCP approximately 25 m below the surface. In addition to measuring currents, the ADCP was also equipped with a fifth central echosounder beam, which measures waves by tracking the water surface, and which can be post-processed to estimate bubble intrusion from breaking waves (Bjørnestad et al., 2025).

2.1.3. Drifters

Numerous drifters, with different capabilities, were deployed at different times during the experiments. In particular, 6 OpenMetBuoys (Rabault et al., 2022) and 2 SFY buoys (Hope et al., 2025) were deployed. These are relatively light and low-cost drogueless drifters developed by MET Norway. They are based on open hardware and software (Cavaleri et al., 2025), and use accelerometers for wave measurements, and global satellite navigation systems for drift tracks. See also Section 2.1 of the Supplementary.

2.2. Oil sampling

Oil was sampled at various times following the release, to document the changes to physical properties over time and provide input to the droplet size model comparison. The measurement of surface thickness and collection of bulk samples are described below.

2.2.1. Surface thickness

Surface thickness was measured by means of pre-weighed 3M Oil Sorbent pads of known area. The pads have hydrophobic and oleophilic properties and will absorb oil, but not significant amounts of water (Fritt-Rasmussen and Brandvik, 2011). These were placed on the oil-covered sea surface, lifted back up, and placed in zip-lock bags to be weighed at a later time. Average oil thickness was calculated from the mass and density of the oil, and the area of the pad. Two example images are shown in Fig. 1, one close to saturation, corresponding to 4.2 mm thickness, and one with only a few isolated specks of oil, corresponding to an average thickness of 0.06 mm. Surface thickness sampling locations were guided by real-time observations from remote sensing, aiming to sample the thickest portions of the oil slick.

2.2.2. Bulk oil samples

Samples of the surface oil were collected by means of a flexible polyethylene cornet bag. Water and oil were scooped up, and the denser water was drained off through the bottom, similarly to a separation funnel (see Fig. S4 in the supplementary). The oil samples were then

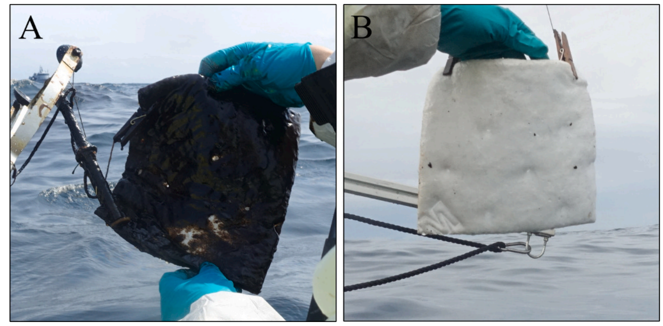

Fig. 1. 3M Oil Sorbent pads during the Oseberg experiment. A) Pad close to saturation 1 h after the release showing a thickness of 4.2 mm. B) Pad with only small amounts of oil after 24 h. In the latter case, the average thickness is 0.06 mm, but note that the oil is mainly confined to a few concentrated specks.

collected in polyethylene sample jars. Water content of the emulsified oil and density of the water-free oil were determined at the time, in the mobile lab aboard NoCGV *Bergen*, while gas chromatography (GC) analysis to determine degree of evaporation and viscosity measurements were conducted later, in the lab at SINTEF.

2.3. Oil droplet measurements

Oil droplet measurements in the water column were based on the SilCam (Silhouette Camera), a camera system developed at SINTEF for the purpose of particle measurements (Davies et al., 2017) in both lab and field. The camera system consists of a standard C-mount CCD camera, fitted with a telecentric lens. The SilCam images a sample volume, which is constrained by a window on the camera side, and by a flat, uniform LED backlight on the far side. Due to the telecentric lens, all particles in the sample volume are in focus, and have the same apparent size regardless of position within the volume, which allows accurate size measurements. Additionally, the known sample volume allows concentrations to be calculated.

Spartacus is a relatively small and light spar buoy, recently developed at SINTEF. It was deployed in a version with two SilCams, at two different depths, as shown in Fig. 2. The body of the buoy is made up of a

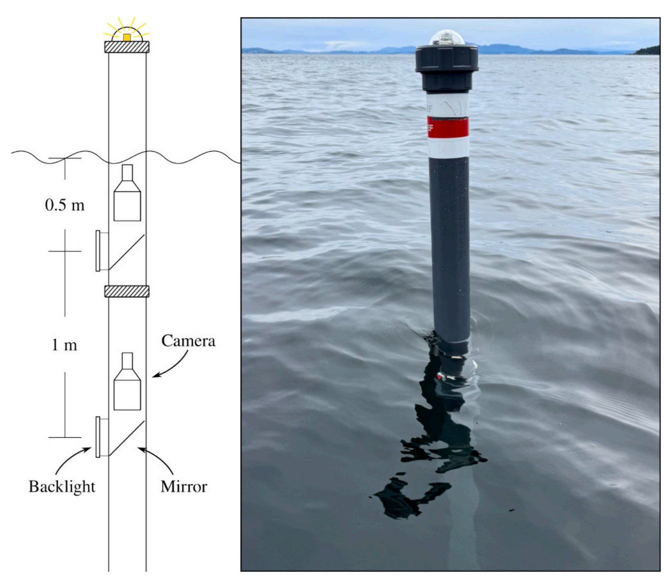

Fig. 2. Schematic illustration of Spartacus with two SilCams, and photo from the Trondheim fjord. The sample volumes are constrained by the windows in the body of the buoy, and the backlights, which are mounted on spacers to maintain a gap of 10 mm. Water can flow freely through the sample volume in the vertical direction.

PVC pressure pipe with an outer diameter of 110 mm, and an inner diameter of about 95 mm. The total length of the body of the buoy is 6 m, and it weighs about 50 kg with instruments, batteries and ballast. The distance between the two cameras is fixed, but the equilibrium depth can be adjusted by adding or removing ballast. The buoy is designed with a long and narrow spar form factor to provide a stable platform for measurements in waves, and to minimally disturb the surface oil slick.

Computers, cameras and lenses are all housed within the main body, with the camera looking horizontally out of the side of the buoy via a 45° mirror and a window, as shown in Fig. 2. The sample volume of the camera is constrained by the flat window which is set into the side of the buoy, and the flat LED backlight. The backlight is mounted on spacers, creating a gap of 10 mm, through which the water can flow freely in the vertical direction. For the SilCam configuration used in Spartacus, the sample volumes were 8 mL per camera, and the image resolution was 13 μm per pixel, which means droplets down to a diameter of around 50–100 μm can be detected and classified. See also Section 2.4 in the Supplementary for additional information.

Processing of SilCam images is done with PyOPIA (Davies et al., 2023), an open-source image processing library developed by SINTEF and others.[3] Images from the SilCam are essentially low-magnification brightfield microscope images, where particles appear dark against a bright background. Briefly, the analysis process consists of contrast adjustment, segmentation into individual particles, classification by a pre-trained convolutional neural network, and size determination from the known pixel size. For the study presented here, all images were stored on disk, and analysed later, using the parallel processing pipeline of PyOPIA.

2.4. Remote sensing

Remote sensing data was collected from vessel-mounted instruments such as oil spill detection radar and infrared cameras, as well as UAVs, manned surveillance aircraft (LN-KYV) and satellites. Measurements were done with electro optical imagery (EO), infrared (IR), and radar. Goals included comparison between the different types of instruments, as well as verifications of the instruments against thickness measured by surface sampling. In addition, remote sensing resources were used to monitor the position, spreading, and drift direction of the oil at all times, with real-time video used to guide the surface sampling.

2.4.1. Radar

Satellites use Synthetic Aperture Radar (SAR), which is an active radar system that transmits signals towards the sea surface and measures the reflected signal. Because it is an active method, using a centimeter-wave source, SAR works during both day and night and through clouds, fog, and rain. Oil on the sea surface can be detected because it dampens capillary waves and short gravity waves (Migliaccio et al., 2015). Normally, these waves reflect radar signals back to the satellite, creating a bright radar image. When oil is present, the surface becomes smoother, reducing the radar backscatter. This appears as dark areas in SAR images, allowing analysts to identify and map potential oil slicks on the ocean surface (Skrunes et al., 2018). It is not generally possible to measure slick thickness by SAR, although this is a topic of ongoing research (Jones, 2023).

The aircraft LN-KYV is fitted with a Terma 9.3 GHz Side-Looking Airborne Radar (SLAR, see, e.g., Gil and Alacid, 2018). Similar to SAR, an oil slick appears dark on a SLAR system due to reduced reflection from small waves, and SLAR can also be used to estimate total area, but not slick thickness. Both SAR and SLAR depend on the natural presence of short waves, and will not work in a complete calm.

Table 1
Bonn Agreement Oil Appearance Code, with thickness categories and corresponding volume of oil per km^2.

Code	Category	Thickness [μm]	Volume per km^2
1	Sheen (silvery/grey)	0.04–0.3	50–300 L
2	Rainbow	0.3–5	300–5000 L
3	Metallic	5–50	5000–50,000 L
4	Discontinuous true oil colour	50–200	50,000–200,000 L
5	Continuous true oil colour	More than 200	More than 200,000 L

2.4.2. Infrared

Infrared sensors detect thermal radiation and measure apparent temperature differences between materials. Oil on the sea surface can be detected because it has different thermal properties than water. During the day, oil absorbs and retains more heat than seawater and therefore appears warmer in infrared images. At night, oil cools down more slowly and can still appear warmer than the surrounding water for some time. It is also possible for oil to appear colder than the surrounding water, due to difference in emissivity or evaporative cooling. These temperature contrasts allow infrared sensors to identify and map oil slicks on the ocean surface under suitable conditions, and can to some degree be used to classify oil according to relative thickness (see, e.g., Leifer et al., 2012), but not measure exact thickness.

2.4.3. Electro optical sensors

Electro optical sensors work with the visible part of the spectrum, and detect reflected sunlight from the sea surface and provide high-resolution images with natural colour information. Oil on the sea surface can be detected because it changes the way light is reflected compared to clean water. Oil slicks may appear as dark, bright, or iridescent features, depending on oil thickness, sun angle, and viewing geometry. The Bonn Agreement Oil Appearance Code (BAOAC) gives a guide for classifying oil slicks into five different thickness categories based on appearance, as shown in Table 1.

2.5. Oils

Two different oils were used in the experiments, MGO and a fresh crude. MGO is classified as a DMA-grade fuel under the ISO 8217:2024 standard,[4] indicating a high-quality distillate marine fuel. It consists of 100% distillate components, has a low viscosity (less than 6 cSt at 40 °C), and is increasingly used in vessels operating in emission-controlled areas, where sulphur limits are typically less than 0.1%. MGO does not form emulsions with water.

Oseberg blend is a light paraffinic crude oil, rich in saturated compounds, with a medium wax content. It is representative of a large group of light paraffinic North Sea oils and has been included in many earlier studies (Faksness et al., 2016) due to being relatively easily available. It was chosen for the current study due to its relatively low viscosity, as it was expected to disperse easily and provide a good target for detection of droplets in the water column.

3. Results and discussion

3.1. MGO experiment

The MGO experiment started with a release of 10 m^3 of marine gas oil between 09:09 and 09:15 on June 6. This corresponds to a release rate of 100 m^3/h, which can occur for example following a collision between two vessels, or a grounding. Environmental conditions are shown in Fig. 3.

The wind speed (10 m elevation) was initially 2–5 m/s, picking up to

[3] https://github.com/SINTEF/pyopia/.

[4] https://www.iso.org/standard/80579.html.

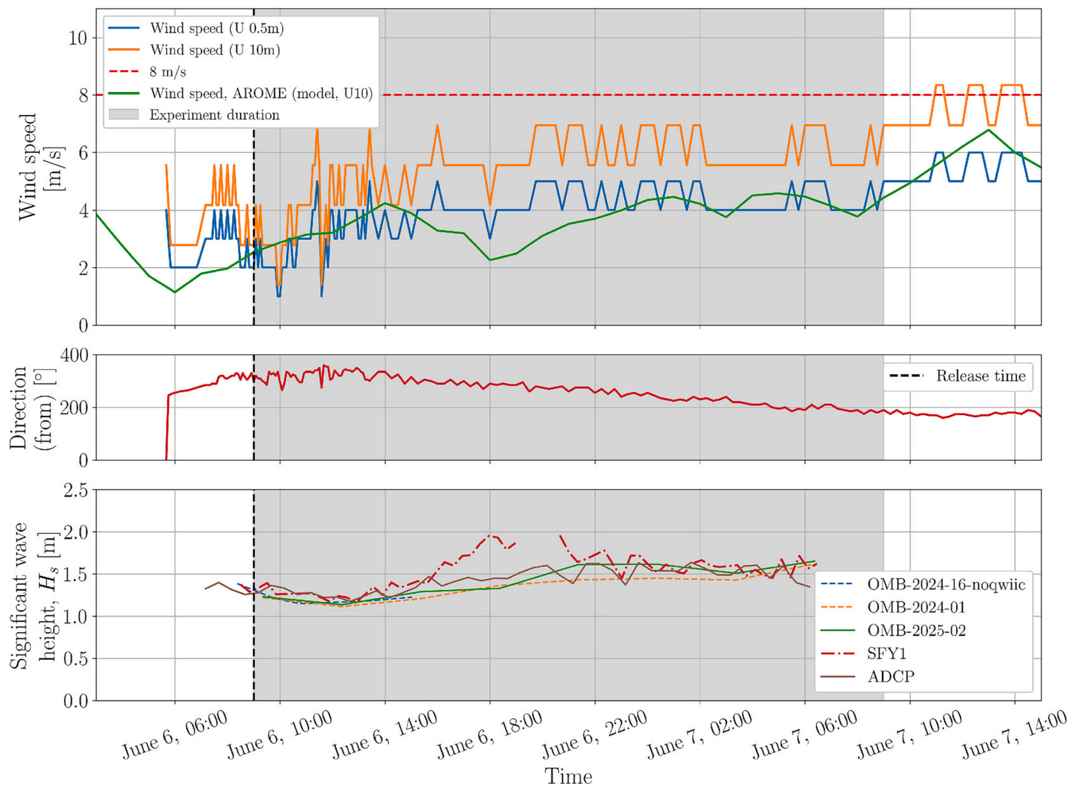

Fig. 3. Environmental conditions during the MGO experiment (grey region). Top panel: Measured wind speed from Sailbuoy (0.5 m elevation, and scaled to 10 m elevation) and modelled wind speed from MET Norway's operational forecast system MEPS. Middle panel: Measured wind direction from Sailbuoy. Bottom panel: Measured significant wave height from drifting buoys and upward-looking ADCP.

6–7 m/s later in the experiment, with little or no breaking waves throughout. Significant wave height was between about 1.2 and 1.6 m, mainly old sea following windy conditions in the days leading up to the experiment. Outlines of the slick based on remote sensing from LN-KYV and UAVs are shown in Fig. 4, together with selected surface sampling locations. The slick outlines from UAVs are based on mosaics of several images, with an example shown in Appendix A, and areal extents are listed in Table 5.

As mentioned earlier, the purpose of this experiment was to investigate the spreading and evaporation of a marine diesel in calm

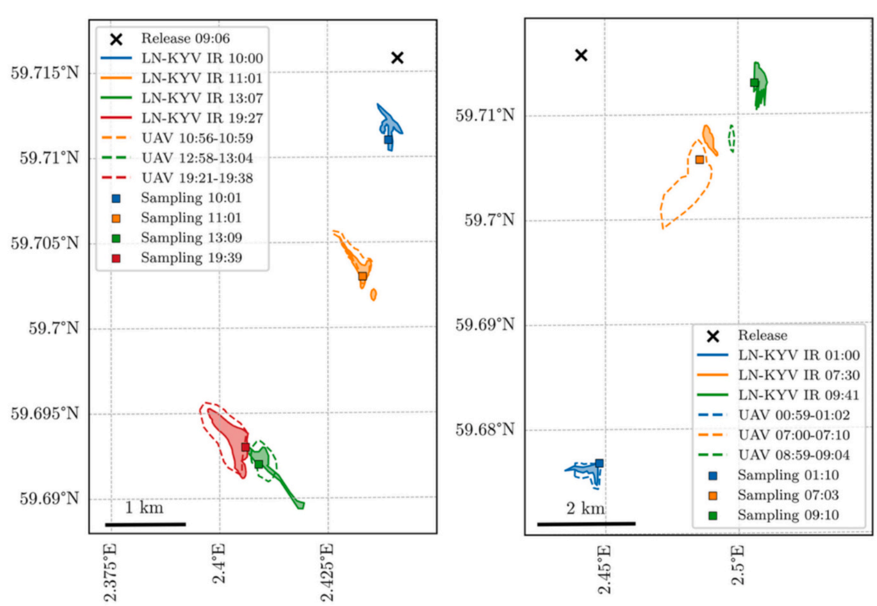

Fig. 4. Outlines of the MGO slick, based on remote sensing from LN-KYV (IR) and UAVs (EO). Left panel shows observations on June 6, right panel on June 7. Also shown are positions of surface thickness samples at corresponding times.

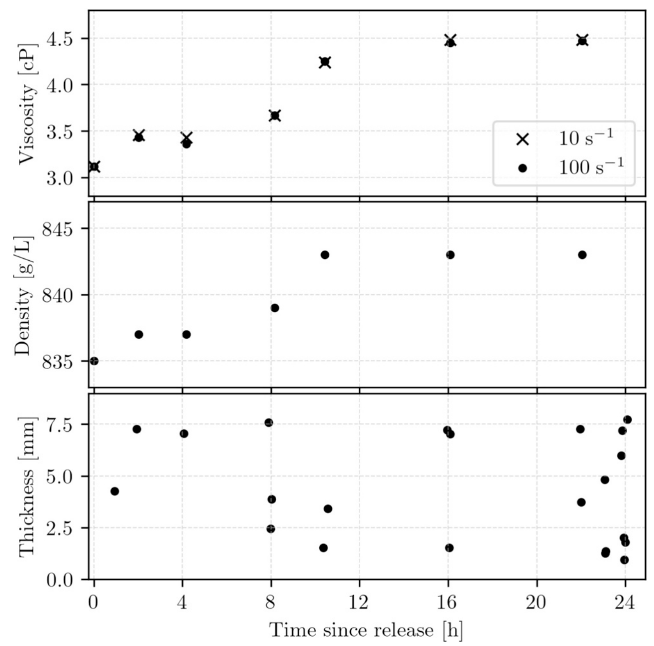

Fig. 5. Viscosity (at two shear rates), density, and slick thickness for the MGO experiment, as a function of time after release. The oil sample for viscosity and density at $t = 0$ was taken prior to release. Water content remained at 0% throughout the experiment.

conditions. For 10 m^3 of MGO spilled in wind speeds below 6–7 m/s, with little or no breaking waves, surface sampling found that the thickest parts of the slick remained at 7–8 mm throughout the 24 h of the experiment, as shown in Fig. 5. Viscosity and density from surface samples are also shown in Fig. 5. The MGO does not form an emulsion, and water content remained at 0% throughout. Viscosity increased only slightly, from 3.12 cP at the outset to 4.47 cP after 22 h. Density changed from 835 g/L to 843 g/L. Very few droplets were detected in the water column.

In breaking wave conditions, spreading and thinning of an oil slick is driven in part by entrainment, shear diffusion and resurfacing (Elliott, 1986), as well as gravity spreading and variations in surface currents. In calm conditions with little or no entrainment, spreading is much slower. The classic treatments of oil spreading on calm waters (Fay, 1971; Hoult, 1972) make a number of idealized assumptions, such as no wind or currents, and constant oil slick thickness. The rate of spreading is then calculated from a balance of forces, such as the hydrostatic pressure within the oil balanced against the drag of the stationary water beneath the oil film.

In our case the slick did not have a constant thickness, but rather consisted of patches of thick oil surrounded by thin oil or sheen. This could have had a retarding effect on gravity spreading, as the surrounding thin oil film could lead to increased drag against the water without being thick enough to contribute significantly to the gravity spreading.

The slick was still relatively intact after 24 h, as seen in the IR image in Fig. 6. However, the increasing scatter in the thickness measurements shown in Fig. 5 towards the end of the experiment reflects that over time the thickest parts of the slick were scattered and covered a smaller area, and became harder to identify during sampling. Despite thicknesses of several millimetres, the MGO slick did not appear as white on IR with white-hot setting, but was detectable as IR cold. We note also that the transparency and weak colour of the MGO made it hard to detect true colour visually, meaning that thickness estimation from EO remote sensing is challenging.

Fig. 6. Aerial IR (white-hot mode) photo of the MGO slick, 24 h after release. The thickest parts of the slick are found near the leading edge (towards the lower right). Photo taken from the surveillance aircraft LN-KYV.

Diesel spilled at sea has generally been assumed to evaporate and disperse relatively quickly in the water masses (see, e.g., comments in report about the Helge Ingstad diesel spill (Boitsov, 2019)). Guidance on diesel spills from NOAA[5] states that diesel "spreads very quickly to a thin film", and a study based on NOAA's model GNOME found that diesel dispersed/evaporated within hours, even at modest wind speeds of 2.5–7.5 m/s (Farzingohar et al., 2024). The current results contradict these assumptions, though they confirm and extend the results from OOW 2022 (Karoliussen et al., 2022).

Evaporation was determined based on GC chromatograms of the bulk samples taken from the surface, and was found to reach 15%–20% after 22 h. However, the samples were taken from the thick parts of the slick, which are expected to show less evaporation than the thinner parts, due to the smaller surface area per volume in the thick parts.

After 24 h, the remaining patches of thick oil were dispersed by the application of surface dispersant (Slickgone NS), and mechanical energy from NoCGV *Bergen*. Further details are given in the supplementary material.

3.2. Oseberg crude oil experiment

The experiment with Oseberg crude oil was intentionally carried out in conditions with more wind and breaking waves, as the main purpose was to study natural entrainment. The experiment started with the release of 10 m^3 of fresh Oseberg Blend between 09:03 and 09:07 on June 8. This corresponds to a release rate of 3600 m^3/day, which is within a realistic range for a hypothetical spill from a platform at the Norwegian continental shelf.

The wind speed (10 m elevation) remained around 10–12 m/s the first 12 h after release, and then died down during the night (see Fig. 7). Significant wave height was measured at about 1.5 m at the start of the experiment, increasing to 2–2.4 m in the late evening before decreasing after midnight to about 1.4–1.8 m the next morning. Outlines of the slick based on remote sensing are shown along with surface sampling locations in Fig. 8, and observations of total area are given in Table 6 in Appendix A.

The main purpose of the experiment was to measure droplets in the water column, as well as oil parameters (thickness, water content, density and viscosity), and meteorological parameters (wind, current, waves). The objective was to capture a sufficiently complete set of data to allow for comparison against models for natural dispersion.

[5] https://response.restoration.noaa.gov/sites/default/files/Small-Diesel-Spills.pdf.

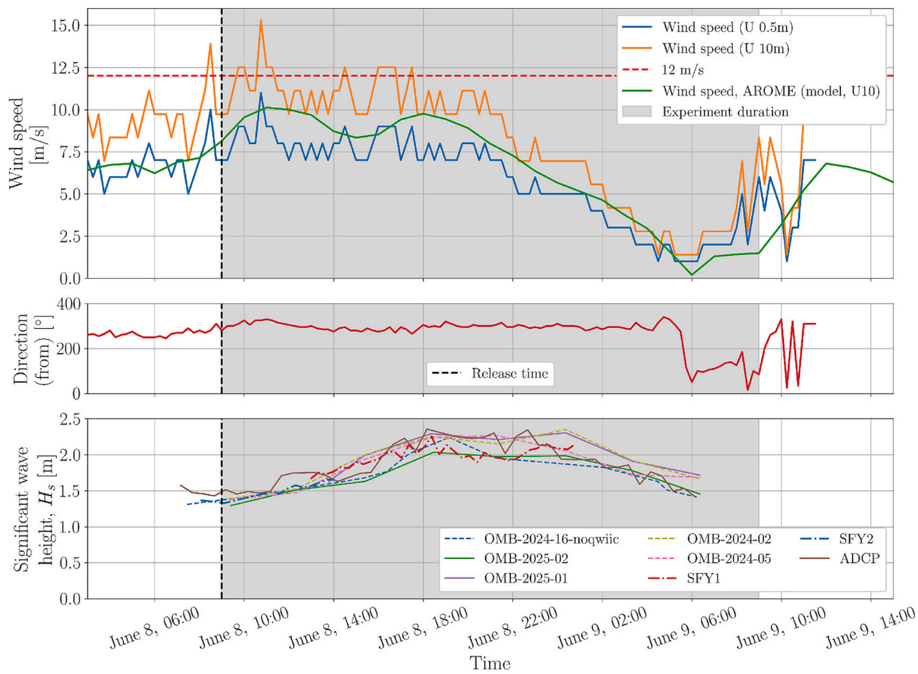

Fig. 7. Environmental conditions during the Oseberg experiment (grey region). Top panel: Measured wind speed from Sailbuoy (0.5 m elevation, and scaled to 10 m elevation) and modelled wind speed from MET Norway's operational forecast system MEPS. Middle panel: Measured wind direction from Sailbuoy. Bottom panel: Measured significant wave height from drifting buoys and upward-looking ADCP.

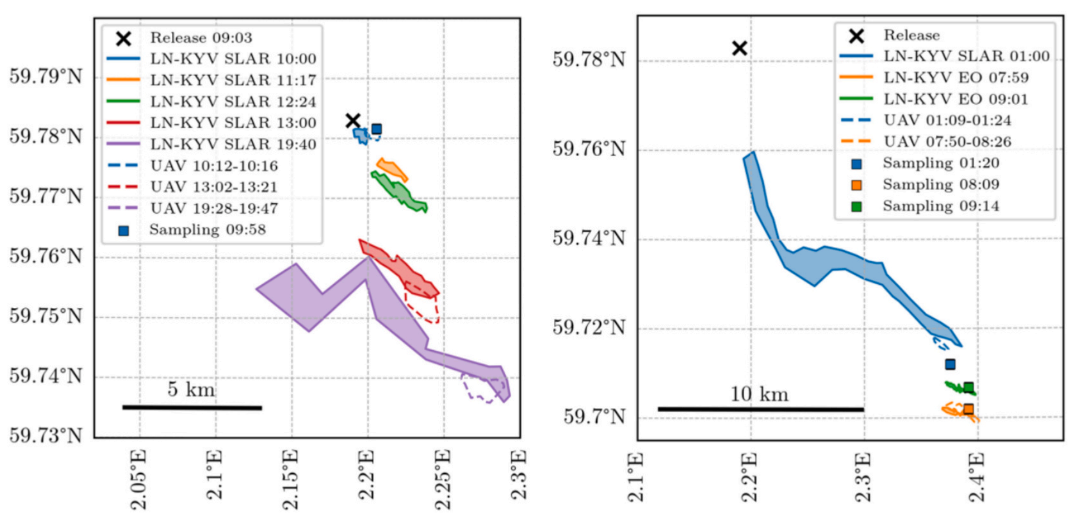

Fig. 8. Outline of Oseberg slick based on remote sensing from LN-KYV (SLAR and EO) and UAVs (EO), and location of surface samples for thickness (June 8 left and June 9 right).

3.2.1. Surface samples

Surface sampling was carried out throughout the experiment. Fig. 9 shows viscosity, water content, density, estimated evaporation, and thickness at different times. Note that relatively unstable emulsions were generated, and viscosity was not measured in the field, but later in the lab at SINTEF, see also additional information in Section S4 of the supplementary. Due to high wind, it was at times not possible to place the 3M sorbent pads correctly on the surface, and no thickness measurements were taken between 13:15 (4 h after release) and 01:20 (16 h after release). In the later samples, continuous thick oil was not visible, and only sheen with interspersed small lumps of oil was found (see Fig. 1). Fig. 10 shows the slick 4 h after release, at 12:59, and Fig. 11 shows the thickest part of the slick 16 h after release, as seen from the LN-KYV.

Due to the wind and wave conditions, the surface oil dispersed relatively quickly, and the last bulk sample of oil was obtained after 11 h. The estimated evaporation shown in Fig. 9 is calculated from the measured density of the water-free oil, by interpolating data on density vs. degree of evaporation based on earlier lab studies.

A very small sample was recovered after 23.5 h, sufficient to obtain a GC chromatogram to estimate evaporation, but not for water content or viscosity. By comparison with GC chromatograms for lab-weathered oils, it was found that the samples taken 8 and 11 h after release were comparable to a residue after heating to 250 °C, or approximately 45% evaporative loss. (GC chromatograms are found in Section S6 in the supplementary.)

Reaching the equivalent of heating to 250 °C after less than 12 h indicates relatively rapid evaporation, as this has previously been said to

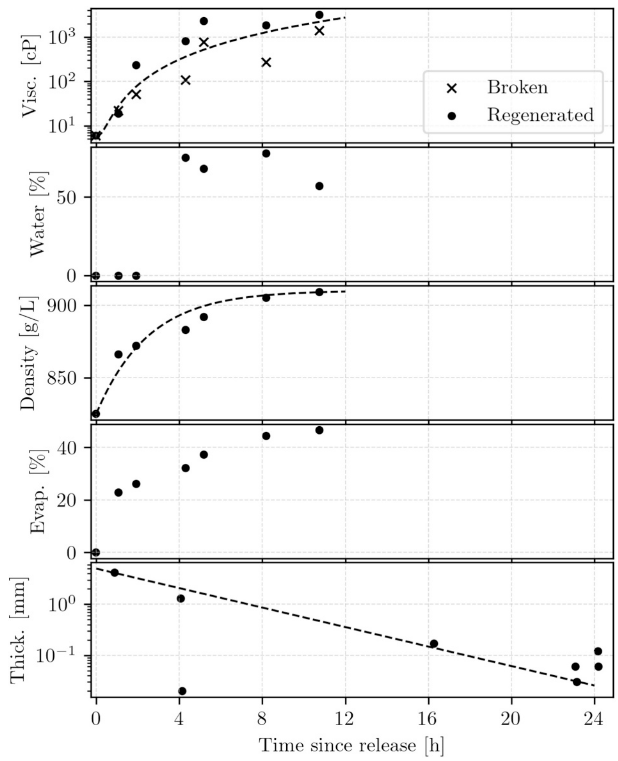

Fig. 9. Viscosity, water content, density, estimated evaporation, and thickness from surface samples of the Oseberg crude. Viscosity was measured later, in the lab at SINTEF, at a shear rate of 10 s^{-1}. Broken refers to measurement of the partially separated emulsion as it was at the time of measurement; regenerated means it has been rotated in a separation funnel overnight, with the same water content. The oil sample for viscosity and density at $t = 0$ was taken prior to release. Evaporation is estimated based on density. The dashed lines are fitted curves used to interpolate the measured values to arbitrary times in the model comparison (Section 4.1).

Fig. 10. IR photo (white-hot mode) of the Oseberg slick 4 h after release, taken from LN-KYV. The white area indicates thicker parts of the slick.

be equivalent to 2–5 days at sea (Daling et al., 1990). After 23.5 h at sea, the evaporative loss is estimated at 60%, and no components below C_{13} were detected in the sample. Sea surface temperatures were approximately 12 °C (see Fig. S3 in the Supplementary).

3.2.2. Droplet size measurements

During the Oseberg experiment, droplet size distributions from natural entrainment were measured. The Spartacus buoy with two integrated SilCams was deployed downwind of the slick. Surface slicks typically drift at about 3.5% of the wind speed (Schwartzberg, 1971; Jones et al., 2016), while Spartacus has considerable drag against the water, and is therefore less affected by the wind than the surface slick. As the oil overtakes and drifts past Spartacus, it essentially completes a transect through the slick. As it emerged from the thinner, more scattered part of the slick, Spartacus was recovered from the water, and repositioned downwind of the thick part of the slick, to complete another transect. The situation is shown schematically in Fig. 12.

Fig. 11. IR photo (white-hot mode) taken from LN-KYV, showing the Oseberg slick and workboat doing surface sampling, 16 h after release. No continuous thick oil was visible at this time.

During the Oseberg experiment, Spartacus was deployed three times, and completed four transects of the slick. Both cameras were recording at 3 frames per second during these deployments, for a total of about 172,000 images. The sample volume is 8 mL per image, for a sample rate of 1.44 L per minute per camera, and in total 1376 L sampled. Two example images from Spartacus are shown in Fig. 13.

Results of the droplet size measurements are shown as functions of time in Fig. 14, showing the 60-s sliding average volume-based median droplet size (d^v_{50}). Also shown is the number of detected droplets per minute, which shows distinct peaks at the times when the thick part of the slick first overtakes Spartacus at the start of each transect.

Due to the relatively high sea state, Camera 1, being at a depth of about 0.5 m in still water (see Fig. 2), was above the surface part of the time, while Camera 2 (depth 1.5 m) would rarely, if ever, be out of the water. Presumably this is the main reason why Camera 2 tends to detect more droplets than Camera 1 (see Fig. 14, particularly Transects 1 and 2). It was also observed that the window of Camera 1 was at times smudged by oil, particularly early in the first transect. Static or slowly changing features in the images, such as an oil smear, are removed by the background correction feature in PyOPIA, but will temporarily affect droplet detection in the obscured part until the oil is washed away.

The shaded intervals shown in Fig. 14 were selected for further analysis, and both volume- and number-based cumulative droplet size distributions were extracted from the data. These are shown in Fig. 15, and the obtained d_{50} values are summarised in Table 2. Table 2 also includes significant wave height and surface oil properties for those intervals when Spartacus was in the thick, leading edge of the slick. Surface oil data for the other intervals is not known, as the surface sampling was targeting the thickest parts of the slick. See Section 5 of the Supplementary material for additional information on the droplet size distributions.

To illustrate the measurement conditions, we show in Fig. 16 the slick and Spartacus in UAV photos taken at 09:21 on June 8, shortly after Spartacus was deployed in the water, and shortly before the leading edge of the slick overtakes Spartacus (the first droplets were detected around 09:22, see Fig. 14). Both EO and IR imagery are shown in Fig. 16, with the IR giving some indication of the variable thickness within the slick, even at this early stage. In Fig. 17, showing photos taken at 09:56, the slick has been drifting past Spartacus for about 35 min. From Fig. 14, we see that number of droplets detected per minute is by then greatly

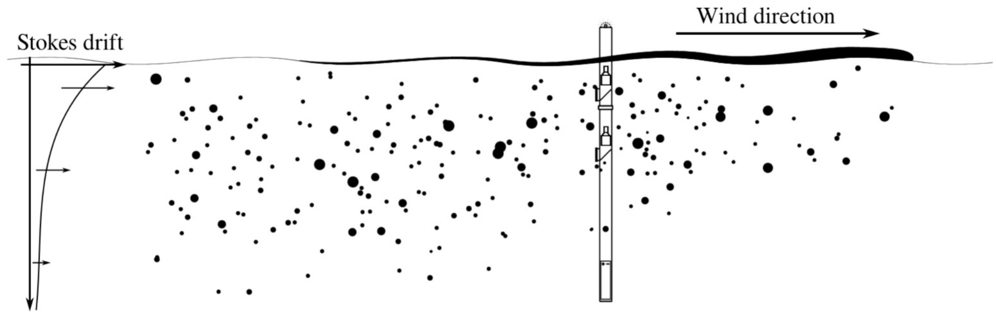

Fig. 12. Spartacus and oil slick shown schematically (not to scale). Surface oil is affected by both wind drag and Stokes drift, and is typically assumed to drift at about 3.5% of the wind speed. The submerged droplets will be less impacted by the Stokes drift and wind-driven currents, and will drift at slower speeds depending on their depths.

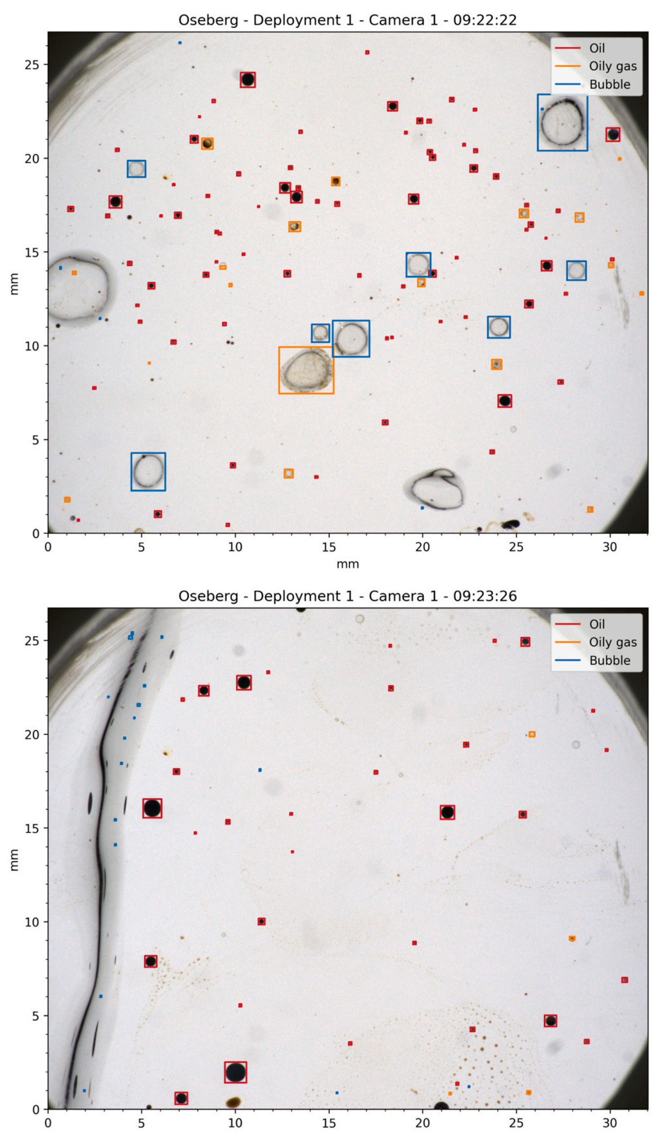

Fig. 13. Images from the upper camera in Spartacus, at the start of the Oseberg experiment. Particle classification from PyOPIA is also shown.

reduced from the high values early in the transect, and the d^v_{50} has been stable at about 300 μm for some time. The droplets detected at this time are likely a combination of locally produced droplets, and droplets from the thicker parts of the slick that remain suspended by turbulence.

4. Evaluation of existing droplet size models

As described above and illustrated in Fig. 12, the droplet size measurements are made in a complex natural environment. The slick, being transported by Stokes drift and wind-driven surface currents, will drift faster than both Spartacus and the submerged droplets, with the thicker parts of the slick at the leading edge downwind (Johansen, 1982; Elliott, 1986; Reed et al., 1994). Spartacus was deployed downwind of the slick, such that the thickest part of the slick would reach Spartacus first. At the start of a transect, Spartacus will therefore tend to encounter locally produced droplets, that are formed by wave breaking in the thickest parts of the slick. Later, as Spartacus is in the middle parts of the slick, the droplets it encounters can come from either upwind or downwind, depending on their depth history.

In what follows, we will present a comparison of the measured droplet sizes during intervals 1a, 2a, and 3a (see Table 2), against droplet sizes predicted by previously published models. The reason for selecting these intervals for the comparison are two-fold: First, given that the slick thickness measurements, as well as the bulk samples taken for oil properties, were all targeting the thickest part of the slick, this is where we have the most representative oil data for a comparison. Second, as discussed above and sketched in Fig. 12, droplets under the leading edge of the slick are likely produced locally, from waves that break in the leading edge, while those under the middle and tail ends of the slick can be from anywhere in the slick. Hence, during the start of each transect, when Spartacus is in the thick, leading edge of the slick, we can reasonably assume to be measuring droplets that are produced locally, from oil with approximately known properties. The relevant oil properties for intervals 1a, 2a, and 3a, interpolated in time by means of the fitted curves shown in Fig. 9 are listed in Table 2, along with significant wave heights.

Droplet measurements taken under the middle and end of the slick should more properly be compared against a full oil spill model, which includes not only the entrainment, but also the vertical and horizontal transport, and resurfacing. In the current study, we limit the scope to only direct comparisons against equilibrium models.

4.1. Existing droplet size models

The existing droplet size prediction models were derived from small-scale laboratory experiments (Delvigne and Sweeney, 1988; Reed et al., 2009; Johansen et al., 2015; Li et al., 2017a; Wang et al., 2024; Mostaani et al., 2026b). All the models we consider here, except the one by Delvigne and Sweeney (1988), express the characteristic droplet size relative to some length scale ℓ as a functional relationship of nondimensional numbers:

$$\frac{d^{n,v}_{50}}{\ell} = \mathscr{F}(\mathrm{We}, \mathrm{Oh}, \mathrm{Vi}) \qquad (1)$$

We note that Eq. (1) is the general case, not all models make use of all

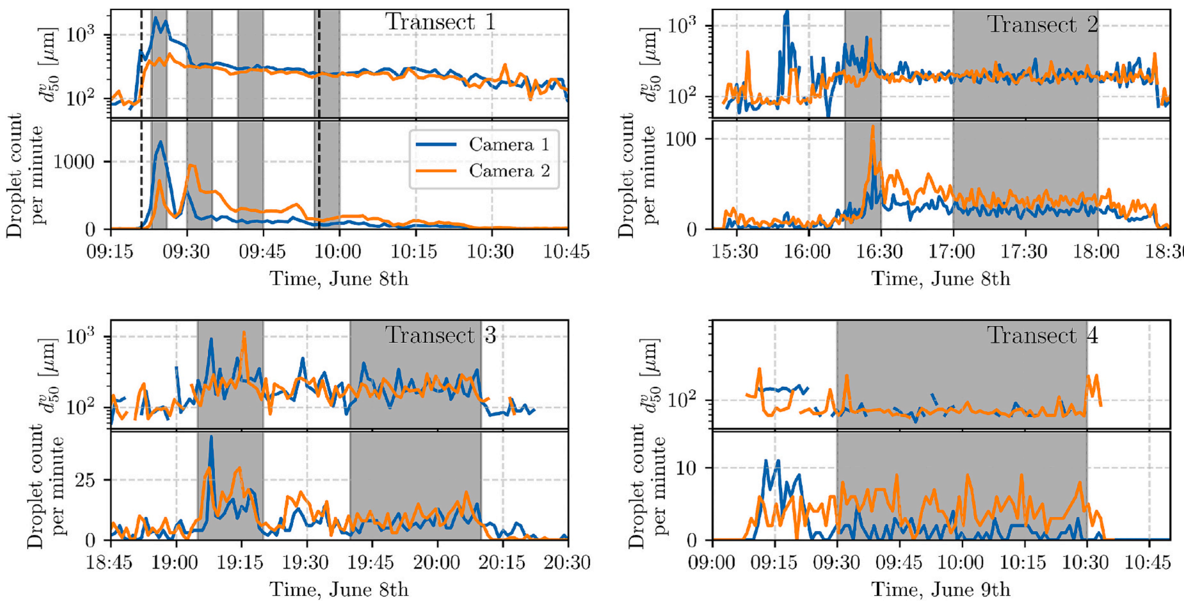

Fig. 14. Measured d_{50}^v(60-second sliding average) and droplet counts from the four transects of Spartacus through the Oseberg slick. The shaded areas correspond to the intervals listed in Table 2, and the dashed black lines for Transect 1 indicate the time of the images shown in Figs. 16 and 17.

the different dimensionless numbers. The Weber, Ohnesorge and Viscosity numbers are defined as

$$\mathrm{We}_o = \frac{\rho_o h_s\, gH_s}{\sigma_{ow}}, \quad \mathrm{We}_{RT} = \frac{\rho_w d_{RT}\, gH_s}{\sigma_{ow}} \tag{2a}$$

$$\mathrm{Oh}_{RT} = \frac{\mu_o}{\sqrt{\rho_o \sigma_{ow} d_{RT}}} \tag{2b}$$

$$\mathrm{Vi}_o = \frac{\mu_o \sqrt{gH_s}}{\sigma_{ow}} \tag{2c}$$

where ρ_o and ρ_w are the densities of oil and water, μ_o is the dynamic viscosity of oil, σ_{ow} is the interfacial tension between oil and water, and H_s is the significant wave height. All the models use a velocity scale $u_\ell \sim \sqrt{gH_s}$, while they differ in their choice of length scale: h_s is the slick thickness, while d_{RT} is the Rayleigh-Taylor droplet diameter, given by

$$d_{RT} = 4 \times \sqrt{\frac{\sigma_{ow}}{(\rho_w - \rho_o)g}}.$$

This is the maximum stable diameter of a droplet rising under its own buoyancy, which is a function of oil density and oil-water interfacial tension.

The main argument for using slick thickness as a length scale is that it has been found experimentally to have an effect on droplet sizes (Johansen et al., 2015; Mostaani et al., 2026b). An effect is also mechanistically plausible, as the breakup of a thin film would be unlikely to create large droplets. The main argument made for using the Rayleigh-Taylor diameter as a length scale, is that the slick thickness is difficult both to measure and to model (Li et al., 2017b), while d_{RT} can be calculated from well-known parameters (density and interfacial tension). Table 3 presents a summary of existing models used to predict measured droplet sizes in the literature.

The model proposed by the seminal experimental study of Delvigne and Sweeney (1988) formulates the (number-based) median droplet size, d_{50}^n, based on oil kinematic viscosity, μ_o/ρ_o, and the mean energy dissipation rate in unit volume of the breaking wave, ε, rather than on nondimensional numbers. According to Delvigne and Sweeney (1988), the energy dissipation rate of breaking waves is on the order of 1000 W/m^3 to 10,000 W/m^3, but no specific parameterisation is given. We assume a linear relationship from start of breaking at 5 m/s to large waves at 20 m/s. Hence, the energy dissipation rate ε is estimated as a function of wind speed as

$$\varepsilon = 600\ \mathrm{J/m^4} \times U_{10} - 2000\ \mathrm{W/m^3}, \tag{4}$$

where U_{10} is the wind speed at 10 m elevation in units of m/s.

The model proposed by Johansen et al. (2015) predicts number-based median droplet size, d_{50}^n, as a function of the Weber and Viscosity numbers. It uses the oil slick thickness, h_s, as the length scale. A variation of the Johansen model has been derived that directly predicts volume-based median diameter, d_{50}^v, which is more useful for use in a Lagrangian oil spill model (Nordam et al., 2019). The functional form is the same as in the model due to Johansen et al. (2015), but the coefficients have been re-fitted to values of d_{50}^v derived from the original dataset (Reed et al., 2009), as well as data from Li et al. (2017a).

The model due to Li et al. (2017b) uses the Rayleigh-Taylor droplet size, d_{RT} as a length scale, and predicts volume-based median droplet size, d_{50}^v, as a function of the Weber and Ohnesorge numbers. A unique feature of this model is that it was derived to predict droplet sizes for both wave entrainment and blowouts (for the blowout case the velocity scale is the exit velocity). It was fitted and validated against data from both wave entrainment and underwater jet releases.

A more recently published model is due to Wang et al. (2024). This model uses the same length and velocity scales as Li et al. (2017b), and also predicts the d_{50}^v as a function of the Weber and Ohnesorge numbers. However, even though the model was fitted to experiments with a single low-viscosity oil, the predicted droplet size is proportional to $\mathrm{Oh}_{RT}^{5.788}$, which gives a *very* strong sensitivity to oil properties. The droplet sizes predicted by this model was in some cases off by many orders of magnitude, hence we have left it out of the detailed comparison.

Finally, we include a model due to Mostaani et al. (2026b). This model uses the slick thickness as length scale, and it predicts d_{50}^v as a function of the Weber and Viscosity numbers. The model coefficients were fitted to data from Reed et al. (2009) and Li et al. (2017a), as well as new experiments presented in Mostaani et al. (2026a, 2026b). We note that the model as formulated in Mostaani et al. (2026b) uses $\sqrt{2gH_s}$ as a velocity scale, while in Table 3 the factor $\sqrt{2}$ has been absorbed into the numerical prefactor to be consistent with the definition of the Weber and Viscosity numbers used by the other models.

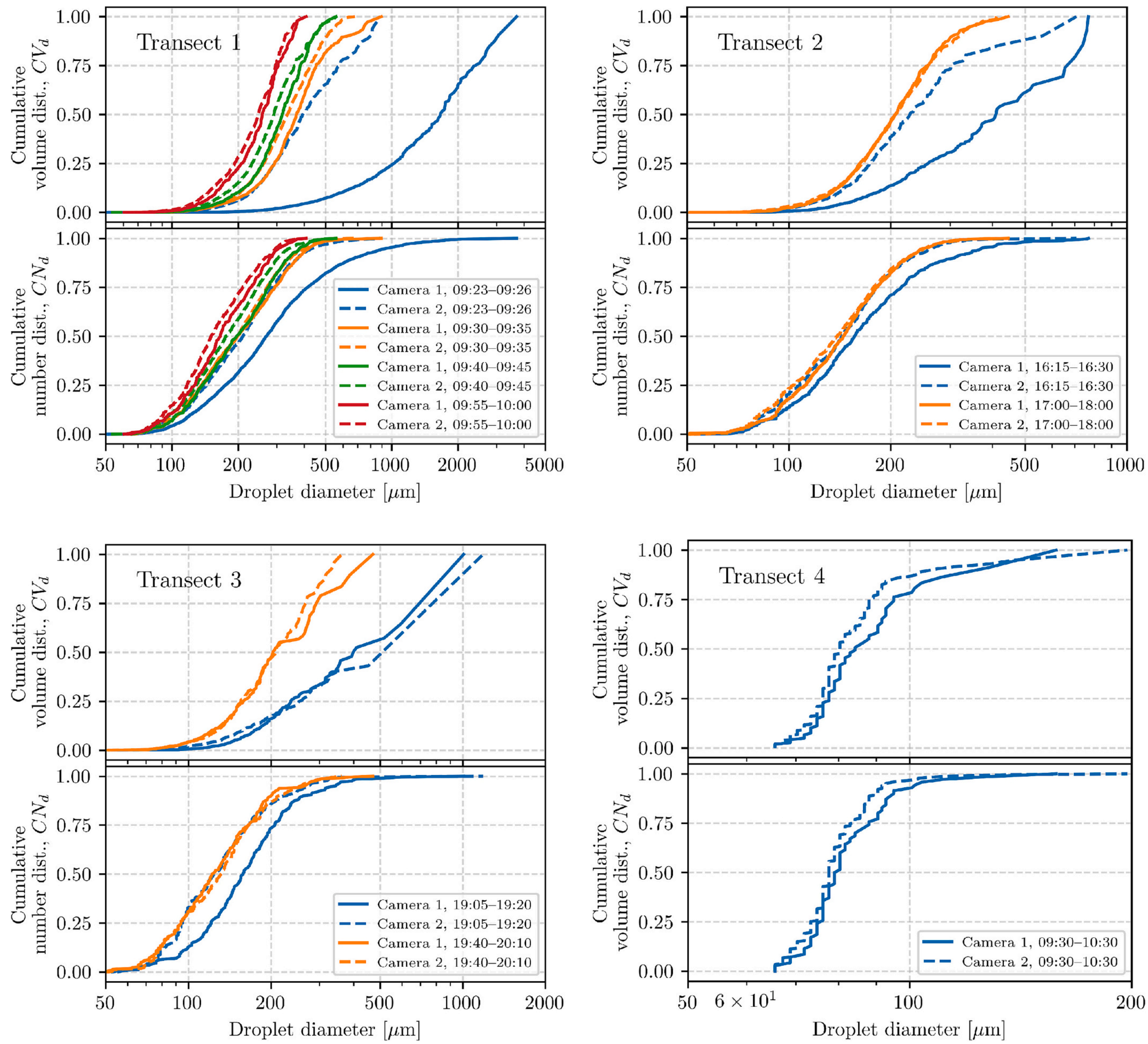

Fig. 15. Cumulative volume distribution and number distribution, for both cameras, at selected intervals (see Fig. 14) during the four transects of Spartacus through the Oseberg slick.

4.2. Comparison of droplet sizes

Fig. 18 shows the measured d_{50}^{n} and d_{50}^{v} from both cameras on Spartacus, during transect intervals 1a, 2a, and 3a (see Fig. 14). Also shown are the predicted characteristic droplet sizes from the different models presented above, based on the oil and wave properties for the relevant times (see Table 2).

The model by Delvigne & Sweeney predicts a characteristic size which is too small for interval 1a, while it is somewhat too large for intervals 2a and 3a. Similarly the model due to Li et al. also shows a trend of increasing droplet sizes from transect 1a to 3a, predicting too small droplets for 1a, and too large for 2a and 3a. We note that neither the Delvigne & Sweeney nor the Li model takes slick thickness into account. This could be a contributing factor to underestimating droplet size for the earliest interval when the oil is fresh but thick, and overestimating in the two later intervals, when the surface oil is weathered but thinner.

The model due to Johansen et al. (2015) predicts a smaller number-based median droplet size than measured in all cases, but it is interesting to note that it closely follows the observed downwards trend from intervals 1a to 3a. In particular, when comparing to the d_{50}^{n} at Camera 2, the original Johansen model is off by an approximately constant factor of 0.45 for all three intervals.

The re-fitted version of the Johansen model, which has been designed to predict d_{50}^{v} directly, performs similarly, showing the same downwards trend as the original model. The downwards trend is less obvious in the measured d_{50}^{v}, but this could be due to the volume distribution being more affected by a few large outlier droplets than the number distribution (see Fig. 15). Finally, the model due to Mostaani et al. (2026b) predicts droplets that are too small in all cases, with no obvious trend across the intervals.

The largest errors are seen for transect 1a, when the oil is thick and the droplets are largest. As noted above, not all models use slick thickness as a parameter. It is also possible that wave damping plays a role for

Table 2
Measured d_{50}^{n} and d_{50}^{v} from Spartacus, and related oil properties and significant wave height at different intervals during the Oseberg experiment. Oil properties are only given for those intervals when Spartacus was in the thickest part of the slick, where surface samples were collected. C1 is Camera 1 (average depth 0.5 m), C2 is Camera 2 (average depth 1.5 m). The numbering refers to different transects, as described in Section 3.2.2 and shown in Fig. 14. The oil-water interfacial tension for Oseberg has previously been measured to 17 mN/m (Brandvik et al., 2023) and is assumed to be relatively unaffected by weathering. Variable notation: h_s is the slick thickness, μ_o is the oil viscosity, ρ_o is the oil density, and H_s is significant wave height.

No.	Time	h_s [mm]	μ_o [cP]	ρ_o [g/L]	H_s [m]	d_{50}^{n} [μm]	d_{50}^{n} [μm]	d_{50}^{v} [μm]	d_{50}^{v} [μm]
						C1	C2	C1	C2
1a	09:23–09:26	5	6.4	832	1.375	277	210	1667	394
1b	09:30–09:35	–	–	–	–	202	199	377	335
1c	09:40–09:45	–	–	–	–	212	176	319	291
1d	09:55–10:00	–	–	–	–	167	150	267	247
2a	16:15–06:30	1.1	946	905	1.85	157	143	411	229
2b	17:00–18:00	–	–	–	–	145	139	207	209
3a	19:05–19:20	0.7	1561	908	2.15	158	124	398	452
3b	19:40–20:10	–	–	–	–	122	131	203	209
4a	09:30–10:30	–	–	–	–	79	78	84	80

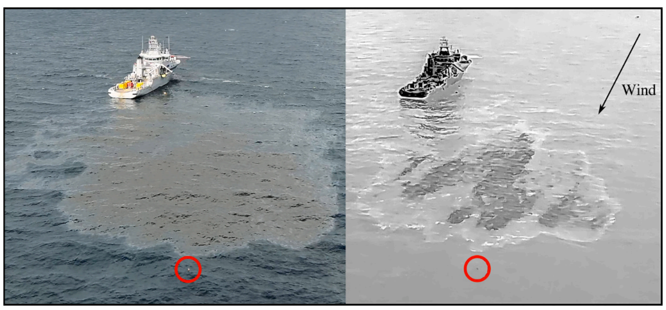

Fig. 16. The Oseberg crude slick, shown in UAV photo from 09:21 on June 8, shortly before the slick overtakes Spartacus (red outline). The EO and IR cameras were mounted on the same UAV. The IR mode is black hot. The arrow shows the approximate direction of wind and wave propagation.

this particular case. As can be seen in Fig. 16, the waves have to propagate through the whole slick before reaching the leading edge, where the droplets are measured. For interval 1a, when the slick is still several millimetres thick and fairly concentrated, this may reduce the probability and intensity of the breaking, and thus give larger droplets than would be predicted from the H_s measured outside the slick.

We note also that the models on average correspond better to the droplet sizes measured by Camera 2. The two cameras in Spartacus sit at different equilibrium depths (0.5 m and 1.5 m). Most lab measurements are made close to the surface, but if we normalise the measurement depth by the wave height, Camera 2 might be more comparable to the lab sample depths.

4.3. Inherent challenges in the model comparison

Given that not all parameters can be controlled and measured as precisely in the field as in the lab, there are some inherent challenges in a model comparison. An obvious and important example is the wave height. In the experiments of Reed et al. (2009), the height is the fall height of water from a tray, onto the oil slick, while in Li et al. (2017a), a breaking wave is generated by a single push by the wave paddle, and the wave height given in the paper is the measured maximum wave height. For the experiments by Mostaani et al. (2026b), breaking waves are generated from a focused wave packet, and measured H_s is used in the model. Focused breakers will (by design) have an unusually high ratio of maximal wave height to significant wave height, as seen for example in Mostaani et al. (2026b) where $H_{\max}$ is 4–5 times higher than H_s. For wind-driven breaking waves in the open ocean, whitecaps form at the crests of waves, and “spill” down the slope of the wave for some distance, hence the water involved in the breaking does not experience a free fall of height equal to the wave height. Therefore, it is not obvious that using $\sqrt{gH_s}$ as a velocity scale is the optimal way of scaling from lab to field. This point applies equally to all the models discussed here, except the one by Delvigne & Sweeney.

Droplet sizes in the lab are measured after a single breaking event interacting with an idealized, uniform-thickness oil slick at a fixed sampling location. Measured droplet sizes in the field cannot be

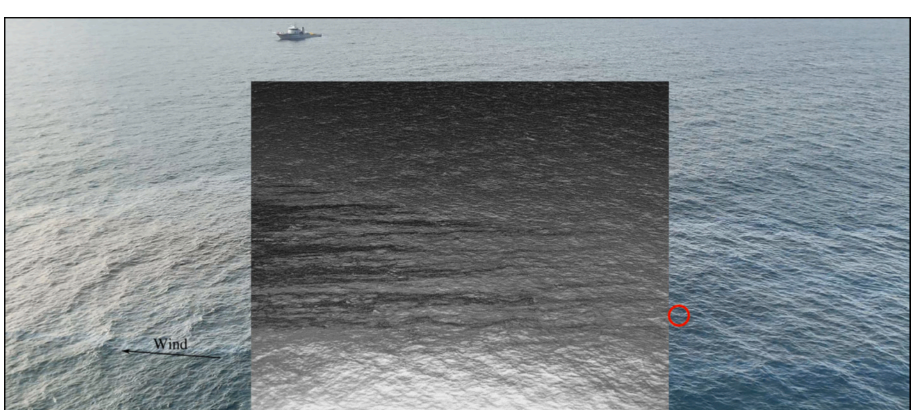

Fig. 17. The Oseberg slick and Spartacus (red outline), shown in UAV photo from 09:56 on June 8. The EO and IR cameras were mounted on the same UAV, and the IR photo has been superimposed on the visible image (which was taken with a more wide-angle lens). The IR mode is black hot. The arrow shows the approximate direction of wind and wave propagation.

Table 3
Summary of existing models for characteristic droplet size in wave entrainment. Variable notation: ℓ is the characteristic length scale, g is acceleration of gravity, H_s is significant wave height, h_s is oil slick thickness, d_{RT} is the Rayleigh-Taylor diameter. In the model of Delvigne & Sweeney, μ_o/ρ_o has units cSt, and ε has units W/m^3.

Authors	ℓ	Nondim. groups	Model
Delvigne & Sweeney	–	–	$d^n_{50} = 1400\,(\mu_o/\rho_o)^{0.34}\varepsilon^{-0.55}$
Johansen et al.	h_s	$\mathrm{We}_o, \mathrm{Vi}_o$	$d^n_{50} = h_s \times 2.251\,\mathrm{We}_o^{-0.6}(1+0.027\,\mathrm{Vi}_o^{0.6})$
Johansen et al. (refit)	h_s	$\mathrm{We}_o, \mathrm{Vi}_o$	$d^v_{50} = h_s \times 7.93\,\mathrm{We}_o^{-0.66}(1+0.023\,\mathrm{Vi}_o^{0.66})$
Li et al.	d_{RT}	$\mathrm{We}_{RT}, \mathrm{Oh}_{RT}$	$d^v_{50} = d_{RT} \times 1.791\,(1+10\,\mathrm{Oh}_{RT})^{0.46}\mathrm{We}_{RT}^{-0.518}$
Wang et al.	d_{RT}	$\mathrm{We}_{RT}, \mathrm{Oh}_{RT}$	$d^v_{50} = d_{RT} \times 61.51\,\mathrm{Oh}_{RT}^{5.788}\mathrm{We}_{RT}^{-1.1033}$
Mostaani et al.	h_s	$\mathrm{We}_o, \mathrm{Vi}_o$	$d^v_{50} = h_s \times 35.37\,\mathrm{We}_o^{-0.88}\,\mathrm{Vi}_o^{0.13}$

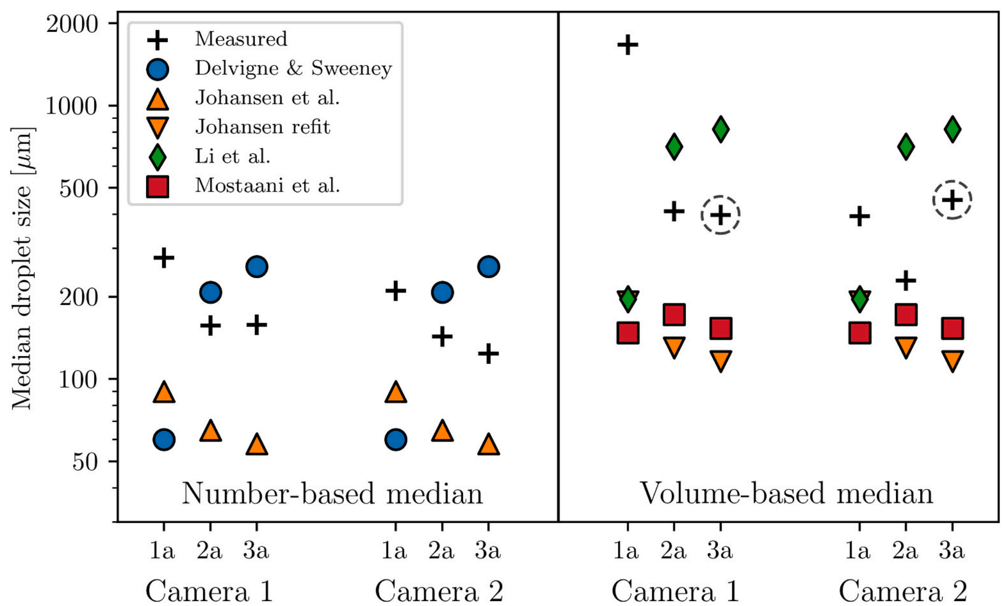

Fig. 18. Performance of existing models (see Table 3) in predicting d^n_{50} (Number-based) and d^v_{50} (Volume-based), at transects 1a, 2a, and 3a with Spartacus during the Oseberg experiment. Note that the model predictions are the same for both Cameras, as depth is not a parameter in the models. The values of d^v_{50} for transect 3a (dashed circles) are probably affected by a few large outlier droplets, as can be seen from the cumulative volume distributions in Fig. 15.

attributed to a single breaking event, but are rather an average over some time interval. As was pointed out in Mostaani et al. (2026a), the median droplet size following a breaking event is reduced as time passes, as the larger droplets resurface faster. Therefore, one might have expected the measured droplet sizes to be consistently smaller than those predicted by models. What was found, however, was that the measured droplet sizes were larger than predicted in most cases.

Finally, the oil slick thickness in the field is nonuniform from the moment it is released and continues to vary as the slick spreads over time, as seen, e.g., in Figs. 10, 16, and 17. In addition, the oil properties evolve, and also the oil water content and viscosity will be spatially heterogeneous. As described earlier, we have performed the model comparison for measurements taken in the leading edge of the slick, where also the surface oil samples were taken, but uncertainties remain.

4.4. Parameter ranges spanned in model development

To evaluate the similarity between the conditions at the large-scale field measurements of the present study and the small-scale laboratory measurements used in the development of the existing models, we present in Table 4 the ranges of the variables and nondimensional groups for the present study, and for the data the different models are based on. The individual experiments from the studies in Table 4 are also shown in Fig. 19, together with the conditions at Transects 1a, 2a, and 3a from the current study.

Perhaps most noteworthy, the significant wave height, H_s, is about an order of magnitude higher for the field measurements than for the laboratory measurements (except for one experiment by Delvigne and Sweeney (1988), though their model is not based directly on that experiment[6]).

Slick thickness at the early stage (interval 1a) was about 5 mm, similar to values reported by Reed et al. (2009). For intervals 2a and 3a, slick thickness was around 1.1–0.7 mm, the same range as Delvigne and Sweeney (1988), and slightly higher than values used by Li et al. (2017a) and Mostaani et al. (2026a). Viscosity and interfacial tension are well within the ranges covered by earlier lab studies.

If we consider the relevant nondimensional numbers individually, the field experiments performed here are within ranges that have been covered in the lab. However, none of the earlier experiments cover the same range in all dimensionless numbers simultaneously. In Fig. 19 we show pairwise scatterplots of the relevant dimensionless numbers for the individual experiments in the earlier studies, as well as for Transects 1a, 2a, and 3a of the current study. First, we note that the strong correlation between the Ohnesorge and Viscosity numbers, $\mathrm{Oh}_{\mathrm{RT}}$ and Vi_o, is due to the fact that they are both linear in the oil viscosity. Viscosity varies by

[6] The characteristic droplet size model of Delvigne and Sweeney (1988) is based on experiments with submerged oil in a turbulence tank, using TKE dissipation as a variable. They also conducted experiments in wave flumes, with wave heights up to 2 m, and stated that turbulence levels were comparable to those in the turbulence tank.

Table 4
Summary of ranges of the variables and nondimensional groups used in previous and current studies. Note that the model of Delvigne & Sweeney is based on turbulence tank experiments, with turbulence levels stated to be comparable to their wave experiments. Variable notation: H_s is significant wave height, h_s is slick thickness, and d_{RT} is the Rayleigh-Taylor diameter.

Authors	H_s [m]	h_s [mm]	d_{RT} [mm]	We_o	We_{RT}	Vi_o	Oh_{RT}
Delvigne & Sweeney	0.1–1.9	0.2–1.2	12–20	14–805	635–12,487	0.34–16	0.02–0.3
Johansen et al.	0.1–0.3	3–15	13–36	161–3163	774–6530	2.5–623	0.1–12.7
Li et al.	0.22–0.29	0.5	1.8–16	50–4456	1710–18,600	0.64–64	0.02–0.54
Mostaani et al.	0.02–0.06	0.04–0.4	11.2	1.5–13.5	288–859	18–32	1.12
Present study (1a)	1.25–1.5	5	12	3001–3601	8890–10,583	1.3–1.45	0.016
Present study (2a)	1.6–2.1	1.1	15	919–1207	14,250–18,704	220–253	2.0
Present study (3a)	2.0–2.3	0.7	15.2	733–844	18,034–20,740	407–436	3.22

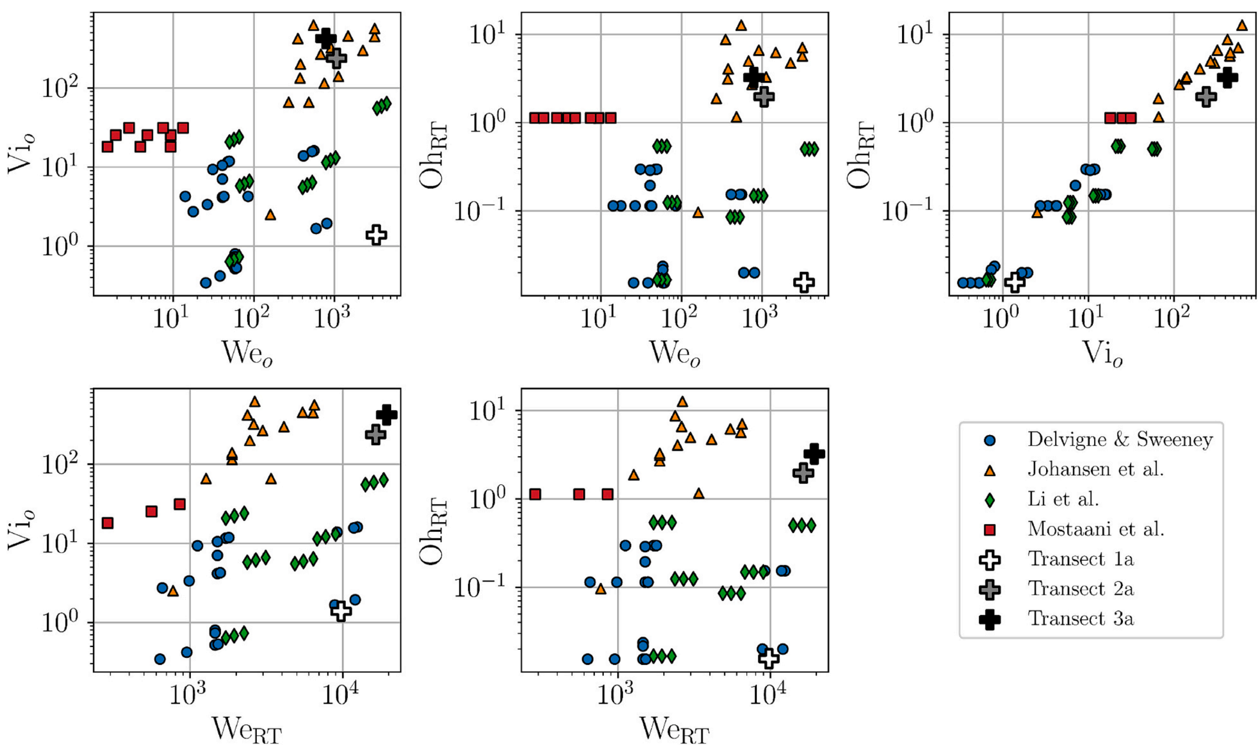

Fig. 19. Distribution of dimensionless numbers used in earlier lab studies, compared to Transects 1a, 2a, and 3a from the current study. See Eqs. (2) for the definitions of the dimensionless numbers.

three orders of magnitude among the studies considered, and thus dominates over variations in the other parameters.

When considering We_o against Oh_{RT} or Vi_o, we see that Transect 1a, only 15–20 min after the release, is placed by itself in the lower right corner. This is due to a combination of the low viscosity of the fresh oil, and the relatively high slick thickness and wave height. Conversely, when considering We_{RT} against Oh_{RT} or Vi_o, we see that Transects 2a and 3a are placed in the upper right corner, also away from the earlier lab experiments. The other experiments with equally high values of We_{RT} are by Li et al., visible as the rightmost cluster of three green diamond markers in the two lower panels of Fig. 19. The three experiments by Li et al. have high values of We_{RT} due to using dispersants to lower the interfacial tension, while for Transects 2a and 3a high values of We_{RT} are mainly due to the large wave height and Rayleigh-Taylor diameter. This places the field experiments in a slightly different regime from the Li experiments, as shown by the difference in Oh_{RT} and Vi_o. Broadly speaking, we can say that the earlier lab studies have spanned field-relevant ranges of the nondimensional numbers used for droplet size models, though the current study does push the boundary a bit for some combinations. We note that most previous lab studies are performed at lower Weber numbers than those that are relevant for natural dispersion of untreated oil in realistic wave heights.

5. Conclusion

Two experimental field releases of oil have been carried out. As these two releases had, for the most part, different scientific objectives, and were carried out with different oils and under different weather conditions, the conclusions are presented separately.

5.1. MGO experiment

A key objective of the MGO experiment was to verify and extend findings from OOW 2022, suggesting that diesel spilled in calm conditions can remain thick for longer than previously thought. The experiment in 2022 (Karoliussen et al., 2022) lasted only 8 h, and one objective was to extend this to 24 h. It was found that 10 m^3 of MGO spilled in calm conditions still showed areas of thick oil even after 24 h, when surface thicknesses up to 8 mm were measured. We conclude that as long as there are no breaking waves, a spill from a light oil such as MGO can remain as a coherent slick with thick patches for at least 24 h.

Remote sensing with IR is more challenging for a transparent oil such as MGO, as it does not absorb as much heat from the sun as a crude oil, and the infrared emissivity is lower. The signature of the MGO slick was mainly found in IR cold, even when surface sampling found the oil to be several millimetres thick.

After 24 h a surface dispersion operation was conducted, where a chemical dispersant (Slickgone NS) was applied from booms mounted on the foredeck of NoCGV *Bergen*. After dispersant application through the thickest parts of the slick, the surveillance aircraft LN-KYV reported no combatable oil visible on the surface, and the experiment was concluded. The conclusion is that the window of opportunity for applying surface dispersants to diesel spills of this size can be at least 24 h, in calm conditions.

5.2. Oseberg crude experiment

The Oseberg experiment was performed in breaking wave conditions, with wind speeds 10–12 m/s. We observed the classic (Johansen, 1982; Elliott, 1986) image of the slick as thick at the leading (downwind) edge, with a large and thin tail formed by resurfacing droplets trailing behind. Evaporation estimated from GC chromatograms was at about 45% after 8 h, comparable to that of a residue after heating to 250 °C in the lab, and after 24 h more than 60% evaporation was estimated. Heating to 250 °C has previously been compared to 2–5 days at sea (Daling et al., 1990), indicating relatively rapid weathering in this case. The Oseberg crude had significant water uptake at the start of the experiment, reaching 75% after 4 h, but the emulsion was unstable. During the surface sampling at 01:20 in the morning of June 9, 16 h after the release, only scattered lumps of oil a few millimetres in size were found, and similarly during surface sampling at 09:14 on June 9 (see Fig. 1).

The most novel aspect of the current study is the measurement of oil droplet size distributions during natural dispersion in the field, made in combination with measurements of oil properties and meteorological and oceanographic observations, including wind and several independent measurements of wave spectra. This allows for the first time a comparison of several existing lab-based droplet size models against field observations. A comparison between measured droplet size distributions, and those predicted by various models, shows some discrepancies, though predictions are generally within a factor of 2–4 from the measured values.

A fundamental difference between the models of Delvigne & Sweeney, and Li et al., compared to the models of Johansen et al., and Mostaani et al., is that the latter use the slick thickness as a length scale. We found that the Delvigne and Li models underestimate the droplet size at the start of the experiment, when the oil is fresh and thick, and overestimates towards the end, when the slick is thinner and the oil more weathered. The Johansen model, on the other hand, closely follows the observed trend of reduced droplet size at the later measurements. This suggests that using slick thickness as a length scale could in principle give better predictive power. However, as pointed out by Li et al. (2017b), slick thickness is challenging to predict, and uncertainty in modelled slick thickness would propagate to uncertainty in modelled droplet size.

Another point, which is common to all the non-dimensional discussed here, is the use of significant wave height as a fall height to derive a velocity scale, $v \sim \sqrt{gH_s}$. Breaking waves in open water are for the most part spilling breakers, and it is not clear that the fall-height approach is the best way to link waves in the lab to waves in the field. Additionally, previous lab experiments have used single waves of a given hight. Waves in the field have random heights, with significant wave height defined as the average height of the 1/3 highest waves.

From our results, it is clear that published droplet size models for natural entrainment have some room for improvement. More research is needed on the validity of scaling from lab to field, and on the choice of length and velocity scales for use in non-dimensional droplet size correlations.

CRediT authorship contribution statement

Tor Nordam: Writing – review & editing, Writing – original draft, Visualization, Supervision, Software, Resources, Project administration, Methodology, Investigation, Formal analysis, Data curation, Conceptualization. **Atle Kleven:** Writing – review & editing, Writing – original draft, Software, Resources, Methodology, Investigation, Formal analysis, Conceptualization. **Frode Leirvik:** Writing – review & editing, Visualization, Resources, Methodology, Investigation, Conceptualization. **Liv-Guri Faksness:** Writing – review & editing, Writing – original draft, Supervision, Project administration, Methodology, Investigation, Conceptualization. **Per Johan Brandvik:** Writing – review & editing, Writing – original draft, Supervision, Methodology, Investigation, Conceptualization. **Jørgen Skancke:** Writing – review & editing, Writing – original draft, Formal analysis, Conceptualization. **Arsalan Mostaani:** Writing – review & editing, Writing – original draft, Visualization, Software, Investigation, Formal analysis. **Gaute Hope:** Writing – review & editing, Writing – original draft, Visualization, Validation, Supervision, Software, Resources, Project administration, Investigation, Data curation, Conceptualization. **Trygve Halsne:** Writing – review & editing, Supervision, Resources, Investigation, Data curation, Conceptualization. **Ingrid C. Taban:** Writing – review & editing, Writing – original draft, Resources, Project administration, Investigation, Funding acquisition, Conceptualization. **Kristin K. Husebye:** Writing – review & editing, Writing – original draft, Methodology, Investigation, Data curation, Conceptualization. **John Inge Karoliussen:** Writing – review & editing, Writing – original draft, Resources, Project administration, Methodology, Funding acquisition, Conceptualization. **Ove Njøten:** Writing – review & editing, Visualization, Methodology, Formal analysis, Conceptualization. **Knut-Frode Dagestad:** Writing – review & editing, Conceptualization. **Lars Robert Hole:** Writing – review & editing, Investigation. **David Peddie:** Writing – review & editing, Resources, Investigation. **Øyvind Breivik:** Writing – review & editing, Supervision, Conceptualization.

Declaration of competing interest

The authors declare that they have no known competing financial interests or personal relationships that could have appeared to influence the work reported in this paper.

Acknowledgements

Oil on water 2025 was conducted and funded by The Norwegian Clean Seas Association for Operating Companies (NOFO) in cooperation with the Norwegian Costal Administration (NCA). This paper was financed by NOFO. The work of Arsalan Mostaani was supported by the Research Council of Norway, through the project ENTIRE (no. 324227). The authors would like to thank the crew on the vessels NoCGV *Bergen* and MS *Sunny Lady*, for their support and hospitality during the field experiments, the laboratory personnel at SINTEF Ocean for their assistance and UAV pilots from Tiepoint, operators from the surveillance aircraft LN-KYV and Kongsberg Satellite Services for their valuable contribution to remote sensing data.

Appendix A. Areal extent of oil slicks

Areal extents of the oil slicks were determined by remote sensing from aircraft (LN-KYV), unmanned aerial vehicles (UAVs), and satellites. Comparisons of the areal estimates are shown for the MGO experiment in Table 5 and for the Oseberg experiment in Table 6. Areal extents from UAVs were based on mosaics of many images, as the UAVs typically did not fly high enough to see the entire slick in one image when looking down. An example mosaic with outlined slick is shown in Fig. 20.

Table 5
Areal extent in m^2 of the MGO slick, determined by remote sensing from aircraft (LN-KYV), unmanned aerial vehicles (UAVs) and satellites. The exact time of each satellite detection is given in the left column, and matched up with the nearest observations from LN-KYV. All times are local (UTC + 2).

	June 6					June 7			
	10:00	11:00	13:00	17:00	19:30	01:00	06:30	09:00	16:26
LN-KYV IR Cold	26,768	28,132	37,503		81,713	44,882	40,000	62,000	
LN-KYV SLAR						905,000	4,199,000	237,700	
UAVs		43,301	59,180	125,634	153,782	101,090	450,085	20,633	
ICEYE 16:55				1,360,000					
RADARSAT-2 19:24					980,000				
RCM-1 19:26					1,730,000				
ICEYE 23:41						600,000			
COSMO-SkyMed 07:15							4,020,000		
ICEYE 16:26									Not visible

Table 6
Areal extent in m^2 of the Oseberg slick, determined by remote sensing from aircraft (LN-KYV), unmanned aerial vehicles (UAVs) and satellites. The exact time of each satellite detection is given in the left column, and matched up with the nearest observations from LN-KYV. All times are local (UTC + 2).

	June 8			June 9		
	10:00	13:00	19:30	01:00	08:00	09:00
LN-KYV IR Hot	3808	11,163	Not visible	Not visible	Not visible	Not visible
LN-KYV IR Cold	42,345	1,131,019	277,000	68,850	Not visible	Not visible
LN-KYV SLAR	105,000	559,000	4,763,000	5,689,000	Not visible	Not visible
UAVs	81,165	542,338	488,602	82,179	256,094	224,357
ICEYE 13:59		2,620,000				
Sentinel-1A 19:35			2,500,000			
RCM-1 19:42			4,310,000			
ICEYE 23:43				8,800,000		
Sentinel-1C 08:11						Not visible

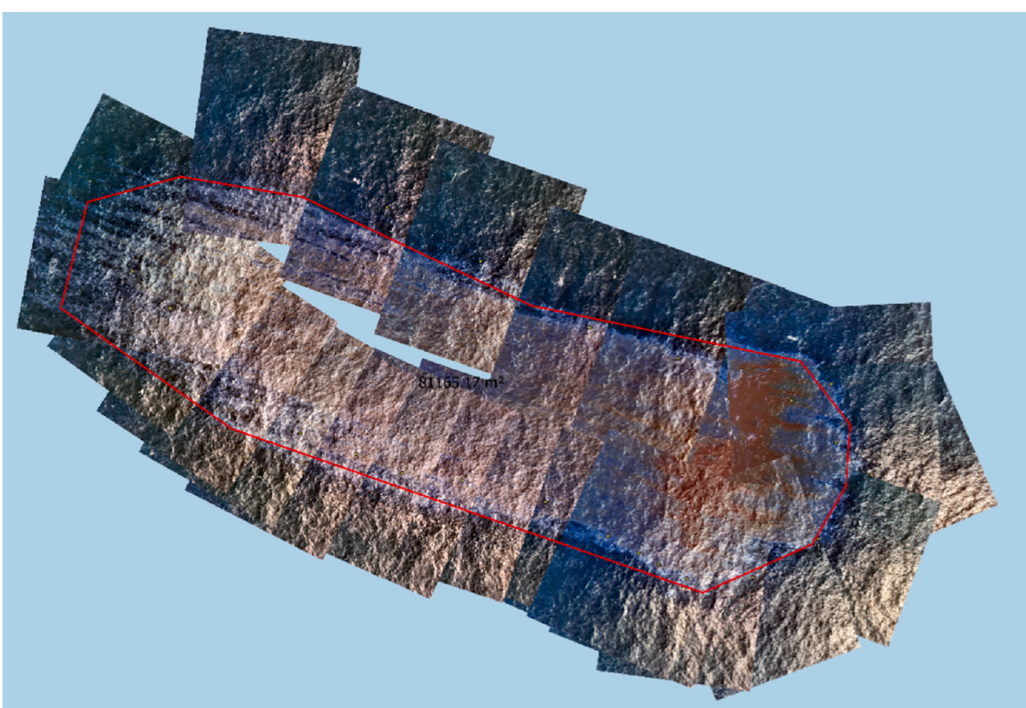

Fig. 20. Mosaic of several images taken from UAVs showing the Oseberg slick at around 10:00 on June 8 (1 h after release). The areal extent is calculated with GIS software from the red outline.

Appendix B. Supplementary data

Supplementary data to this article can be found online at https://doi.org/10.1016/j.marpolbul.2026.119812.

Data availability

Data will be made available on request.

References

Aamo, O.M., Reed, M., Lewis, A., 1997. Regional contingency planning using the OSCAR oil spill contingency and response model. In: Proceedings of the 20th AMOP Technical Seminar, 1, pp. 289–308.

Barker, C.H., Kourafalou, V.H., Beegle-Krause, C.J., Boufadel, M., Bourassa, M.A., Buschang, S.G., Androulidakis, Y., Chassignet, E.P., Dagestad, K.-F., Danmeier, D.G., Dissanayake, A.L., Galt, J.A., Jacobs, G., Marcotte, G., Özgökmen, T., Pinardi, N., Schiller, R.V., Socolofsky, S.A., Thrift-Viveros, D., Zelenke, B., Zhang, A., Zheng, Y., 2020. Progress in operational modelling in support of oil spill response. J. Mar. Sci. Eng. 8 (9), 668.

Bjørnestad, M., Halsne, T., Malila, M., Benetazzo, A., Bergamasco, F., Pistellato, M., Callaghan, A.H., Davison, S., Peach, J., Broström, G., Breivik, Ø., 2025. Whitecaps, bubbles and advection: Insights from concurrent measurements in the open ocean. Geophys. Res. Lett. 52 (21), e2025GL117684.

Boitsov, S., 2019. Oljeforurensning i Hjeltefjorden etter forliset av. KNM «Helge Ingstad». HI-rapport 2019-24.

Brandvik, P.J., Leirvik, F., Hofstad, K.H., McKeever, T.J., 2023. Simulating dispersion of oils from a subsea release comparing mechanical and chemically enhanced dispersion—an experimental study of the influence of oil properties. Mar. Pollut. Bull. 195, 115479.

Brekke, C., Espeseth, M.M., Dagestad, K.F., Röhrs, J., Hole, L.R., Reigber, A., 2021. Integrated analysis of multisensor datasets and oil drift simulations—a free-floating oil experiment in the open ocean. J. Geophys. Res. Oceans 126 (1), e2020JC016499.

Cavaleri, L., Alari, V., Benetazzo, A., Björkqvist, J.V., Breivik, Ø., Davis, J., Hope, G., Kleven, A., Leirvik, F., Nordam, T., et al., 2025. More room at the top: How small buoys help reveal the detailed dynamics of the air–sea interface. Bull. Am. Meteorol. Soc. 106, E1063–E1076.

Cormack, D., Nichols, J.A., 1977. The concentrations of oil in sea water resulting from natural and chemically induced dispersion of oil slicks. In: International Oil Spill Conference Proceedings, Vol. 1977, No. 1. American Petroleum Institute, pp. 381–385.

Daling, P.S., Strøm, T., 1999. Weathering of oils at sea: model/field data comparisons. Spill Sci. Technol. Bull. 5 (1), 63–74.

Daling, P.S., Brandvik, P.J., Mackay, D., Johansen, O., 1990. Characterization of crude oils for environmental purposes. Oil Chem. Pollut. 7 (3), 199–224.

Daling, P.S., Singsaas, I., Reed, M., Hansen, O., 2002. Experiences in dispersant treatment of experimental oil spills. Spill Sci. Technol. Bull. 7 (5–6), 201–213.

Daling, P.S., Moldestad, M.Ø., Johansen, Ø., Lewis, A., Rødal, J., 2003. Norwegian testing of emulsion properties at sea—the importance of oil type and release conditions. Spill Sci. Technol. Bull. 8 (2), 123–136.

Davies, E.J., Brandvik, P.J., Leirvik, F., Nepstad, R., 2017. The use of wide-band transmittance imaging to size and classify suspended particulate matter in seawater. Mar. Pollut. Bull. 115, 105–114.

Davies, E., Nimmo-Smith, A., Nepstad, R., Nordam, T., Brönner, U., Steinvik, A., Giering, S., Masoudi, M., Liu, Z., H'elaoüet, P., Cursons, K., Rau, M., Song, Y., Mostaani, A., Barstein, K., Buscombe, D., 2023. Pyopia: a python Ocean particle image analysis toolbox. In: Proceedings of Particles in Europe (PiE). Heraklion, Crete, pp. 29–36.

Delvigne, G.A., 1985. Experiments on natural and chemical dispersion of oil in laboratory and field circumstances. In: International Oil Spill Conference Proceedings, Vol. 1985, No. 1. American Petroleum Institute, pp. 507–514.

Delvigne, G.A.L., Sweeney, C., 1988. Natural dispersion of oil. Oil Chem. Pollut. 4, 281–310.

Elliott, A.J., 1986. Shear diffusion and the spread of oil in the surface layers of the North sea. Deutsche Hydrographische Zeitschrift 39, 113–137.

Faksness, L.G., Brandvik, P.J., Daae, R.L., Leirvik, F., Børseth, J.F., 2011. Large-scale oil-in-ice experiment in the Barents Sea: monitoring of oil in water and MetOcean interactions. Mar. Pollut. Bull. 62 (5), 976–984.

Faksness, L.G., Brandvik, P.J., Daling, P.S., Singsaas, I., Sørstrøm, S.E., 2016. The value of offshore field experiments in oil spill technology development for Norwegian waters. Mar. Pollut. Bull. 111, 402–410.

Farzingohar, M., Bagheri, M., Gholami, I., Ibrahim, Z.Z., Akhir, M.F., 2024. Mapping pollution dynamics: utilizing GNOME to model oil spill trajectories in tanker terminals. Environ. Sci. Pollut. Res. 31 (25), 37404–37427.

Fay, J.A., 1971, June. Physical processes in the spread of oil on a water surface. In: International Oil Spill Conference Proceedings, Vol. 1971, No. 1. American Petroleum Institute, pp. 463–467.

Fritt-Rasmussen, J., Brandvik, P.J., 2011. Measuring ignitability for in situ burning of oil spills weathered under arctic conditions: from laboratory studies to large-scale field experiments. Mar. Pollut. Bull. 62, 1780–1785.

Frøysa, H.G., Nepstad, R., Sørhus, E., Donald, C.E., Meier, S., Vikebø, F.B., 2025. Oil droplets are severely overlooked in risk assessments. Commun. Earth Environ. 6 (1), 837.

Genders, S., 1988. In-situ detection and tracking of oil in the water column. Oil Chem. Pollut. 4 (2), 113–126.

Gil, P., Alacid, B., 2018. Oil spill detection in terma-side-looking airborne radar images using image features and region segmentation. Sensors 18 (1), 151.

Gros, J., Nabi, D., Würz, B., Wick, L.Y., Brussaard, C.P., Huisman, J., van der Meer, J.R., Reddy, C.M., Arey, J.S., 2014. First day of an oil spill on the open sea: early mass transfers of hydrocarbons to air and water. Environ. Sci. Technol. 48 (16), 9400–9411.

Harrison, W., Winnik, M.A., Kwong, P.T., Mackay, D., 1975. Crude oil spills. Disappearance of aromatic and aliphatic components from small sea-surface slicks. Environ. Sci. Technol. 9 (3), 231–234.

Hole, L.R., Fer, I., Peddie, D., 2016. Directional wave measurements using an autonomous vessel. Ocean Dynam. 66 (9), 1087–1098.

Hope, G., Seldal, T.I., Rabault, J., Bryhni, H.T., Bohlinger, P., Björkqvist, J.V., Nordam, T., Kleven, A., Mostaani, A., Furevik, B.R., et al., 2025. SFY—a lightweight, high-frequency, and phase-resolving wave buoy for coastal waters. J. Atmos. Oceanic Tech. 42, 133–154.

Hoult, D.P., 1972. Oil spreading on the sea. Annu. Rev. Fluid Mech. 4 (1), 341–368.

Jensen, H.V., Andersen, J.H., Daling, P.S., Nøst, E., 2008. Recent experience from multiple remote sensing and monitoring to improve oil spill response operations. In: International Oil Spill Conference Proceedings, Vol. 2008, No. 1. American Petroleum Institute, pp. 407–412.

Johansen, O., 1982. Dispersion of oil from drifting slicks. Spill Technol. Newsl. 134, 370.

Johansen, Ø., Reed, M., Bodsberg, N.R., 2015. Natural dispersion revisited. Mar. Pollut. Bull. 93, 20–26.

Jones, C.E., 2023. An automated algorithm for calculating the ocean contrast in support of oil spill response. Mar. Pollut. Bull. 191, 114952.

Jones, C.E., Dagestad, K.F., Breivik, Ø., Holt, B., Röhrs, J., Christensen, K.H., Espeseth, M., Brekke, C., Skrunes, S., 2016. Measurement and modelling of oil slick transport. J. Geophys. Res. Oceans 121 (10), 7759–7775.

Karoliussen, J.I., Taban, I.C., Engen, F., Frost, B.R., Dale, K., 2022. Olje på vann 2022. Technical Report. NOFO report no. 56053, v1, dated 30.09.22 (in Norwegian).

Keramea, P., Spanoudaki, K., Zodiatis, G., Gikas, G., Sylaios, G., 2021. Oil spill modelling: a critical review on current trends, perspectives, and challenges. J. Mar. Sci. Eng. 9 (2), 181.

Leifer, I., Lehr, W.J., Simecek-Beatty, D., Bradley, E., Clark, R., Dennison, P., Hu, Y., Matheson, S., Jones, C.E., Holt, B., Reif, M., Roberts, D.A., Svejkovsky, J., Swayze, G., Wozencraft, J., 2012. State of the art satellite and airborne marine oil spill remote sensing: Application to the BP Deepwater Horizon oil spill. Remote Sens. Environ. 124, 185–209.

Li, C., Miller, J., Wang, J., Koley, S., Katz, J., 2017a. Size distribution and dispersion of droplets generated by impingement of breaking waves on oil slicks. J. Geophys. Res. Oceans 122, 7938–7957.

Li, Z., Spaulding, M., McCay, D.F., Crowley, D., Payne, J.R., 2017b. Development of a unified oil droplet size distribution model with application to surface breaking waves and subsea blowout releases considering dispersant effects. Mar. Pollut. Bull. 114, 247–257.

Liu, Y., Weisberg, R.H., Hu, C., Zheng, L., 2011. Trajectory forecast as a rapid response to the Deepwater Horizon oil spill. In: *Monitoring and Modelling the Deepwater Horizon Oil Spill: A Record-Breaking Enterprise, Geophys. Monogr.* Ser, 195, pp. 153–165.

Lunel, T., 1993. Dispersion: oil droplet size measurements at sea. In: International Oil Spill Conference Proceedings, Vol. 1993, No. 1. American Petroleum Institute, pp. 794–795.

Migliaccio, M., Nunziata, F., Buono, A., 2015. SAR polarimetry for sea oil slick observation. Int. J. Remote Sens. 36 (12), 3243–3273.

Mostaani, A., Nordam, T., Davies, E.J., Nepstad, R., Skancke, J., Dissanayake, A.L., Leirvik, F., Pettersen, T.A., Barker, C.H., Breivik, Ø., 2026a. Evolution of oil droplet size distributions entrained by breaking waves. Mar. Pollut. Bull. 222, 118665.

Mostaani, A., Nordam, T., Davies, E.J., Nepstad, R., Skancke, J., Dissanayake, A.L., Leirvik, F., Pettersen, T.A., Breivik, Ø., 2026b. Modelling characteristic size distribution parameters of oil droplets generated by breaking waves. Mar. Pollut. Bull. 226, 119420.

Nordam, T., Dunnebier, D.A., Beegle-Krause, C.J., Reed, M., Slagstad, D., 2017. Impact of climate change and seasonal trends on the fate of Arctic oil spills. Ambio 46 (Suppl. 3), 442–452.

Nordam, T., Nepstad, R., Litzler, E., Röhrs, J., 2019. On the use of random walk schemes in oil spill modelling. Mar. Pollut. Bull. 146, 631–638.

Nordam, T., Lofthus, S., Brakstad, O.G., 2020. Modelling biodegradation of crude oil components at low temperatures. Chemosphere 254, 126836.

Price, J.M., Johnson, W.R., Marshall, C.F., Ji, Z.G., Rainey, G.B., 2003. Overview of the oil spill risk analysis (OSRA) model for environmental impact assessment. Spill Sci. Technol. Bull. 8 (5–6), 529–533.

Rabault, J., Nose, T., Hope, G., Müller, M., Breivik, Ø., Voermans, J., Hole, L.R., Bohlinger, P., Waseda, T., Kodaira, T., et al., 2022. Openmetbuoyv2021: an easy-to-build, affordable, customizable, open-source instrument for oceanographic measurements of drift and waves in sea ice and the open ocean. Geosciences 12, 110.

Reed, M., Turner, C., Odulo, A., 1994. The role of wind and emulsification in modelling oil spill and surface drifter trajectories. Spill Sci. Technol. Bull. 1 (2), 143–157.
Reed, M., Singsaas, I., Daling, P.S., Faksnes, L.G., Brakstad, O.G., Hetland, B.A., Hofatad, J.N., 2001. Modelling the water-accommodated fraction in OSCAR2000. In: International Oil Spill Conference Proceedings, Vol. 2001, No. 2. American Petroleum Institute, pp. 1083–1091.
Reed, M., Johansen, O., Leirvik, F., Brørs, B., 2009. Numerical algorithm to compute the effects of breaking waves on surface oil spilled at sea. In: Final Report Submitted to the Coastal Response Research Center 10968, 131.
Röhrs, J., Dagestad, K.F., Asbjørnsen, H., Nordam, T., Skancke, J., Jones, C.E., Brekke, C., 2018. The effect of vertical mixing on the horizontal drift of oil spills. Ocean Sci. 14 (6), 1581–1601.
Schwartzberg, Henry G., 1971. The movement of oil spills. In: International Oil Spill Conference Proceedings, vol. 1971, no. 1. American Petroleum Institute, pp. 489–494.
Skrunes, S., Brekke, C., Jones, C.E., Espeseth, M.M., Holt, B., 2018. Effect of wind direction and incidence angle on polarimetric SAR observations of slicked and unslicked sea surfaces. Remote Sens. Environ. 213, 73–91.
Taban, I.C., Husebye, K.K., Njøten, O., Karoliussen, J.I., 2025. Olje på vann 2025. NOFO Report (63264).
Wang, C., Han, L., Zhang, Y., Jiang, A., Niu, X., 2024. Impact of wave action on the entrainment rate and droplet size of oil. Appl. Ocean Res. 149, 104051.